Research Square

Preprints are preliminary reports that have not undergone peer review.
They should not be considered conclusive, used to inform clinical practice,
or referenced by the media as validated information.

Multi-omics analyses reveal hypoxia-induced CHD2 as a key driver of malignant progression and microenvironment remodeling in HCC via the TGF-β/SMAD axis

YICHEN YANG
First Affiliated Hospital of Xi'an Jiaotong University
Ren Bingyi
First Affiliated Hospital of Xi'an Jiaotong University
Sheng Kai
First Affiliated Hospital of Xi'an Jiaotong University
Bai Zhiyuan
The First Hospital of Yulin
Ren Yang
First Affiliated Hospital of Xi'an Jiaotong University
Yi Lv
First Affiliated Hospital of Xi'an Jiaotong University
Liu Kang
kangliu@xjtu.edu.cn

First Affiliated Hospital of Xi'an Jiaotong University

Research Article

Keywords: Hepatocellular carcinoma, CHD2, HIF1-α, TGF-β/SMAD, tumor immune microenvironment, PD-L1

Posted Date: September 22nd, 2026

DOI: https://doi.org/10.21203/rs.3.rs-11113324/v1

License: This work is licensed under a Creative Commons Attribution 4.0 International License.
Read Full License

Additional Declarations: The authors declare no competing interests.

Multi-omics analyses reveal hypoxia-induced CHD2 as a key driver of malignant progression and microenvironment remodeling in HCC via the TGF-β/SMAD axis

Yichen Yang[1,2†], Bingyi Ren[1,2†], Kai Sheng[1,2†], Zhiyuan Bai[1,3], Yang Ren[1], Yi Lv[1,2], Kang Liu[1,2*]

1. Department of Hepatobiliary Surgery, First Affiliated Hospital of Xi'an Jiaotong University, Xi'an 710061, Shaanxi Province, China.
2. National Local Joint Engineering Research Center for Precision Surgery and Regenerative Medicine, First Affiliated Hospital of Xi'an Jiaotong University, Xi'an 710061, Shaanxi Province, China.
3. Department of General Surgery, First Hospital of Yulin, Yulin 719000, Shaanxi Province, China.

Correspondence: Kang Liu, Department of Hepatobiliary Surgery, First Affiliated Hospital of Xi'an Jiaotong University, Xi'an 710061, Shaanxi Province, China. (E-Mail: kangliu@xjtu.edu.cn)

Keywords: Hepatocellular carcinoma; CHD2; HIF1-α; TGF-β/SMAD; tumor immune microenvironment; PD-L1

†These authors contributed equally to this work.

Abstract

Hepatocellular carcinoma (HCC) is characterized by remarkable molecular heterogeneity. However, the role of the chromodomain helicase DNA-binding protein 2 (CHD2) in HCC remains unclear. This study aimed to explore the biological functions and molecular mechanisms of CHD2 in HCC progression.Multi-omics datasets, including RNA-seq, single-cell RNA sequencing (scRNA-seq), and spatial transcriptomics were integrated with experimental validation to analyze the expression, biological significance and regulatory mechanisms of CHD2 in HCC. CHD2 was upregulated in HCC tissues and was associated with poor survival. Single-cell and spatial transcriptomic analyses demonstrated that CHD2 was enriched in tumor cells and positively associated with an immunosuppressive microenvironment and activation of the TGF-β/SMAD pathway. Mechanistically, HIF1-α directly activated CHD2 transcription under hypoxia. Functional experiments further showed that CHD2 promoted HCC cell proliferation, invasion, and epithelial-mesenchymal transition (EMT), while enhancing PD-L1 expression through activating the TGF-β/SMAD pathway. Our study demonstrates for the first time that CHD2 is a hypoxia-induced oncogenic factor that promotes malignant progression and immune evasion in HCC through activating the TGF-β/SMAD pathway. CHD2 may serve as a promising biomarker and potential therapeutic target for HCC.

Introduction

Hepatocellular carcinoma (HCC) remains a formidable health burden worldwide. It is now the sixth most common cancer and the third leading cause of cancer-related deaths worldwide. The etiology of HCC is generally categorized into viral and non-viral factors (including alcohol-related or metabolic drivers). Notably, in Western countries, while the incidence of HBV/HCV-related HCC has begun to decline due to the widespread implementation of hepatitis B vaccination and the availability of potent antiviral therapies, metabolic-associated steatotic liver disease (MASLD) now plays a key role in driving HCC[1, 2]. HCC shows several typical cancer features, including continued proliferation, induced angiogenesis, and immune evasion. Targeted inhibition of these features has significantly improved survival outcomes. For instance, the combination of immune checkpoint inhibitors with anti-angiogenic drugs, exemplified by atezolizumab plus bevacizumab, has significantly improved overall survival for advanced in advanced HCC patients, with overall suivival between 16 and 23 months[3, 4]. However, HCC exhibits molecular heterogeneity, leading to distinct variations in treatment response and disease progression patterns among individuals. In general, the prognosis of HCC ramains poor.

CHD2 belongs to the chromodomain helicase DNA-binding protein family (CHD). It is an ATP-dependent chromatin remodeler, and it participates in multiple nuclear processes,including transcriptional regulation and DNA repair. Structurally, the N-terminal chromodomains of CHD2 mediate auto-inhibition and chromatin targeting, while its C-terminal DNA-binding domain (DBD) is responsible for DNA length sensing and enzymatic activation, ultimately facilitating the assembly of periodic nucleosome arrays[5]. Recent studies have suggested the oncogenic roles of CHD2 in other cancers. For example, CHD2 can be recruited by FOSL1 to activate neurogenic genes such as EPHB3 and ERBB3, thereby maintaining functional synaptic connectivity between glioma cells and neurons to drive tumor progression[6]. Furthermore, CHD2 has been found to maintain the self-renewal of mouse spermatogonial stem cells by modulating both chromatin accessibility and mRNA stability, marking it as an important protein in spermatogenesis[7]. Despite its established importance in these contexts, the role and underlying regulatory mechanisms of CHD2 in HCC remain largely unknown, needing further investigation.

The TGF-β/SMAD pathway is a canonical pathway that plays an important role in HCC development and progression[8]. Among the identified TGF-β isoforms, TGF-β1 and TGF-β3 are mainly expressed in mammalian cells. As the most extensively studied member, TGF-β1 is closely associated with poor prognosis in various cancers, including HCC[9], bladder cancer[10], and breast cancer[11]. SMAD proteins serve as the central transducers of this signaling cascade, with eight distinct members identified in mammals. The TGF-β/SMAD pathway plays a dual role in oncogenesis. In the early stages of tumor development, it typically suppresses tumor formation by inducing apoptosis and inhibiting cellular proliferation[8, 12]. However, during advanced stages, the pathway undergoes a

functional switch to promote tumor progression by orchestrating epithelial-mesenchymal transition (EMT), stimulating angiogenesis, and facilitating immune evasion.

HCC cells exhibit high metabolic activity coupled with aberrant angiogenesis, which inevitably creates a hypoxic tumor microenvironment (TME) that facilitates the stabilization of hypoxia-inducible factor 1-alpha (HIF1-α). Upon translocation into the nucleus, HIF1-α dimerizes with HIF1-β to form a functional transcriptional complex. This heterodimer subsequently binds to hypoxia-response elements (HREs) that are located in the promoter regions of target genes, thereby initiating the transcription of a diverse array of downstream effectors[13]. HIF1-α acts as a key regulator of multiple phenotypes in HCC, including angiogenesis, invasion, metastasis, immune evasion, and metabolic reprogramming. Despite its established importance, the downstream regulatory landscape of HIF1-α remains incompletely understood, and the identification of novel target genes is vital to fully understand the progression of HCC.

In this study, we systematically evaluated the functional significance of CHD2 in HCC through integrated multi-omics analyses and experimental validation. Leveraging multiple bulk RNA-seq datasets and spatial transcriptomics, we characterized the expression profile and the spatial distribution of CHD2 in HCC. Single-cell RNA sequencing (scRNA-seq) analysis further revealed that CHD2 is intrinsically linked to the remodeling of the immunosuppressive TME. Pathway enrichment analyses indicated a correlation between CHD2 and the activation of the TGF-β/SMAD pathway. Mechanistically, we identified HIF-1α as a direct upstream transcriptional activator of CHD2. Functional assays found that CHD2 promotes tumor cell proliferation, invasion, and EMT. Ultimately, Experimental validation demonstrated that the HIF-1α/CHD2 axis modulates PD-L1 expression and oncogenic phenotypes via the activation of TGF-β/SMAD signaling. In conclusion, our findings highlight CHD2 as a critical regulator of HCC progression and immune evasion, suggesting it could be a promising biomarker and a therapeutic target.

Materials and methods

Data Collection and Sources

Transcriptomic profiles and corresponding clinical metadata for the TCGA-LIHC cohort were downloaded from the Genomic Data Commons (GDC) portal (https://portal.gdc.cancer.gov/), comprising 374 HCC samples and 50 adjacent normal samples. The expression data were utilized in transcripts per million (TPM). Additional HCC patient datasets were obtained from the Integrated Hepatocellular Carcinoma Archive (IHGA)(https://www.hccdatasph.cn/app/ihga), which curates over 100 independent HCC datasets, including the ICGC-LIRI-JP project and 87 GEO datasets, encompassing more than 10,000 tissue samples. Protein expression levels of CHD2 were downloaded from the Clinical Proteomic Tumor Analysis Consortium (CPTAC) (https://proteomics.cancer.gov/data-portal), featuring 165 primary tumor samples and corresponding

normal samples. Immunohistochemistry (IHC) images and CHD2 expression across pcancer cell lines were sourced from the Human Protein Atlas (HPA)(https://www.proteinatlas.org/). Baseline expression levels of CHD2 in healthy tissues were characterized using bulk RNA-seq and scRNA-seq datasets from the GTEx (https://www.gtexportal.org/home/). For single-cell transcriptomic analysis, the HCC scRNA-seq datasets GSE166635 and GSE146115 were analyzed. Spatial transcriptomics data were derived from the study by Yao Liu et al[14]. ChIP-seq dataset for HIF-1α of HepG2 cells under hypoxia was obtained from GSE16347, while hypoxia-induced RNA-seq datasets of HepG2 and Hep3B cells were aggregated from GSE18494, GSE57613, GSE283995, and GSE41666.

Expression and Survival Prognosis Analysis

For the TCGA-LIHC cohort, transcriptomic data were transformed using $\log_2(TPM+1)$ transformation. The differential expression of CHD2 between tumor and normal samples was evaluated using the Wilcoxon rank-sum test. To assess the diagnostic performance of CHD2 in HCC and pan-cancer, Receiver Operating Characteristic (ROC) curves were generated using the pROC package, with the Area Under the Curve (AUC) and 95% confidence intervals (CI) calculated via the DeLong method. Patients were categorized into CHD2-high and CHD2-low expression groups based on the median value of CHD2 expression. Kaplan-Meier curves were plotted using the survival and survminer packages to compare overall survival (OS), progression-free survival (PFS), and disease-specific survival (DSS) between the two groups, with significance determined by the log-rank test. Furthermore, a univariate Cox proportional hazards regression analysis was used to calculate risk scores, and the ggrisk package was used to visualize the distribution of risk scores, survival status, and CHD2 expression. To investigate the correlation between CHD2 and clinicopathological features, donut charts were generated using the ggplot2 package to visualize the proportional distribution of clinical variables across the high- and low-expression groups. Statistical significance across subgroups, including TNM stage, gender, and immune subtypes (C1-C6) by Thorsson et al[15], was analyzed using the chi-square test, Fisher's exact test, or Kruskal-Wallis test as appropriate.

Immune Infiltration and TME Analysis

To evaluate the association between CHD2 expression and immune cell infiltration, multiple deconvolution algorithms, including CIBERSORT[16], xCell[17], MCP-counter[18], quanTIseq[19], and EPIC[20], were employed. The ESTIMATE algorithm was utilized to calculate TME-related scores, specifically the StromalScore, ImmuneScore, and ESTIMATEScore. Spearman correlation analysis was performed to explore the relationship between CHD2 expression and various immune parameters, including 18 immune features[15], 68 immune signatures[21], and 150 immunomodulatory genes associated with five functional categories (chemokines, receptors, MHC, immunoinhibitors, and immunostimulators) from the TISIDB (http://cis.hku.hk/TISIDB/download.php). Significant differences in immune infiltration levels, TME scores, immune-related molecules between CHD2-high and CHD2-low expression groups were visualized using violin plots and heatmap.

The Tracking Tumor Immunophenotype (TIP) database (https://biocc.hrbmu.edu.cn/TIP/) was utilized to assess the activity of the seven-step cancer-immunity cycle. Spearman correlation were conducted to evaluate the association between CHD2 expression and TIP scores, with visualization performed using the linkET R package.

Patients were stratified into quartiles (Q1–Q4) based on CHD2 expression to generate heatmaps illustrating the crosstalk between CHD2 levels, immunomodulators, and genomic status scores.

scRNA-seq Data Processing and Analysis

The scRNA-seq data were processed and analyzed using the Seurat package (v5.4.0). Cells with fewer than 200 detected genes, more than 6,000 detected genes, mitochondrial transcript proportions exceeding 15%, or fewer than 500 UMIs were excluded during quality control. Following normalization and scaling, highly variable genes (HVGs) were identified for subsequent analysis. Principal Component Analysis (PCA) was employed to reduce dimensions, and batch effects across different samples were mitigated using the Harmony algorithm. Cells were then clustered via an unsupervised approach based on a Shared Nearest Neighbor (SNN) graph and visualized using the Uniform Manifold Approximation and Projection (UMAP) to assess the distribution of CHD2 expression.

To evaluate the enrichment of CHD2, cells were stratified into CHD2-positive ($CHD2^+$) and CHD2-negative ($CHD2^-$) groups based on its expression. The proportional distribution of cell subtypes was compared between these groups, and the Kruskal-Wallis test was used to assess the statistical significance of CHD2 expression differences across clusters.

Cell-cell communication analysis was conducted using the CellChat package. Ligand-receptor interaction networks were constructed to compare the interaction strengths of $CHD2^+$ and $CHD2^-$ malignant cells with other cell populations. Additionally, the major incoming and outgoing signaling patterns across cell groups were identified. To further explore mechanistic links, the expression of CHD2 was co-visualized with key components of the TGF-β/SMAD pathway (TGFB1, TGFB3, SMAD2, and SMAD3) and HIF1-α on UMAP embeddings, with their correlations quantified via Spearman correlation analysis. Finally, the Variance-adjusted Mahalanobis (VAM) algorithm was utilized to estimate activity scores of the TGF-β/SMAD [22] and HIF/Hypoxia[23] pathways at single-cell resolution, followed by spatial visualization on the UMAP embeddings.

Spatial Transcriptomics Data Analysis

Spatial transcriptomic analysis of HCC tissue sections was performed using data downloaded from the Sparkle database(https://www.grswsci.top). To resolve the cellular composition of each spatial spot, we employed the Cottrazm spatial deconvolution algorithm. Subsequently, spatial domains were defined based on the estimated malignant cell fraction. Spots with a malignant cell proportion greater than zero were classified as malignant regions (Mal), while others were designated as non-malignant regions

(nMal). Differential expression analysis was then conducted to compare CHD2 levels between these two regions.

The SpatialFeaturePlot function from the Seurat package was utilized for the in situ visualization of CHD2 expression within the tissue architecture. Furthermore, the VAM algorithm was applied to score and visualize the spatial activity patterns of the TGF-β/SMAD and HIF/Hypoxia signaling pathways. Finally, Spearman correlation analysis was performed to evaluate the association between CHD2 expression levels and the relative proportions of various cell types at each spatial location.

Methylation Modifications and Genomic Instability

This study used the Sangerbox (http://sangerbox.com/essay.html) comprehensive bioinformatics platform to investigate the genetic and epigenetic characteristics of CHD2. First, the RNA methylation modification levels of CHD2 and the methylation status of individual CpG sites within the promoter region were analyzed. Subsequently, to assess the impact of CHD2 on genomic stability, the correlation between CHD2 expression and Loss of Heterozygosity (LOH) scores in a pan-cancer context was calculated. In terms of mutational landscape, waterfall plots of the top 15 genes with the highest mutation frequency in the CHD2-high and CHD2-low expression groups were generated to visualize the genomic variation characteristics under different expression backgrounds.

In addition, we used the TIMER database (https://compbio.cn/timer1/) to evaluate the relationship between CHD2 gene copy number variation (CNV) and immune cell infiltration levels. The analysis focused on the differences in the immune infiltration of B cells, CD8+ T cells, CD4+ T cells, macrophages, neutrophils, and dendritic cells under different CNV states.

Drug Sensitivity Analysis

We calculated the Spearman correlation between CHD2 expression and drug sensitivity across four databases: GDSC1, GDSC2 (https://www.cancerrxgene.org/), CTRP (https://portals.broadinstitute.org/ctrp/), and PRISM (https://portals.broadinstitute.org/ctrp/). To explore therapeutic strategies that could counteract the pro-oncogenic effects mediated by CHD2, we performed signature matching for 1,288 compounds in the cMAP database (https://www.broadinstitute.org/connectivity-map-cmap) using the XSum algorithm to calculate similarity scores. Based on the comparison between patients with high and low CHD2 expression, the top 150 up-regulated and down-regulated genes were respectively selected to construct the gene signature for screening potential small-molecule drugs[24, 25].

In silico Knockout and Genome-wide CRISPR-Cas9 Screening via DepMap

The scRNA-seq dataset GSE146115 was processed using the Seurat R package for data normalization. Cell type were annotated based on marker genes. To delineate the regulatory impact of CHD2, we performed an in silico knockout analysis using the scTenifoldKnk framework (v1.0.3). An expression matrix comprising CHD2 and the top 2,000 HVGs was constructed. The algorithm generated 10

subnetworks, with 300 cells randomly sampled per subnetwork to assess perturbations in the gene regulatory network (GRN). Significantly differentially regulated genes (DRGs) were identified based on an adjusted p-value (p.adj < 0.05). The regulatory shifts, quantified by fold change and Z-score, were visualized using volcano and bar plots[26].

To further evaluate the functional essentiality of CHD2 across various cancers, genome-wide CRISPR-Cas9 screening data were retrieved from the DepMap portal(https://depmap.org/portal/download/). The CERES algorithm was employed to calculate gene dependency scores for approximately 17,000 genes. Since lower CERES scores indicate a higher degree of gene essentiality, the top 200 cell lines exhibiting the highest dependency on CHD2 were identified[27].

Enrichment Analysis and PPI Network Construction

Differentially expressed genes (DEGs) between CHD2-high and CHD2-low expression groups were identified using the limma package (v3.64.3), with thresholds of $|\log_2 FC| > 1$ and FDR < 0.05. Volcano plots were generated using ggplot2 (v4.0.2) to visualize the distribution of DEGs. To explore the potential biological functions and signaling pathways involved, we performed Gene Ontology (GO) and Kyoto Encyclopedia of Genes and Genomes (KEGG) enrichment analyses. Gene Set Enrichment Analysis (GSEA) was conducted using the clusterProfiler package, referencing the "h.all.v2026.1.Hs.symbols.gmt" hallmark gene set from MSigDB. Normalized Enrichment Scores (NES) were calculated for each gene set. Furthermore, Gene Set Variation Analysis (GSVA) was employed to score 14 functional states derived from the CancerSEA database. Pathway activity levels were quantified using the Z-score, and Spearman correlation was applied to evaluate the association between CHD2 expression and these functional indices. Finally, a protein-protein interaction (PPI) network was constructed by integrating data retrieved from the ComPPI (https://comppi.linkgroup.hu/) and GeneMANIA (http://genemania.org) databases.

ChIP-seq Peak Annotation and Gene Association

Genomic annotation of the HIF-1α ChIP-seq peaks was performed using the ChIPseeker package (v1.46.1). The promoter region was defined as the sequence within ±2 kb of the transcription start site (TSS). Through this approach, peaks were assigned to specific functional genomic features, including promoters, exons, introns, and distal intergenic regions, to identify potential regulatory targets. Furthermore, the seq2gene function was employed to link peak sites to proximal or overlapping genes.

Cell Culture and Treatment

The human normal liver cell line THLE-2 and HCC cell lines (Huh7, HCCLM3, PLC/PRF/5, HLF, SNU-449, and Hep3B) were purchased from Immocell. Cells were cultured in DMEM,1640 or BEGM medium supplemented with 10% fetal bovine serum (FBS; Gibco) and 1% penicillin-streptomycin (Invitrogen) at 37°C in a humidified atmosphere containing 5% CO_2. For hypoxia exposure, cells were placed in a modular incubator chamber (Thermo Scientific) maintained at 1% O_2. The TGF-β/SMAD

pathway inhibitor Vactosertib (HY-19928; MCE) was used.

Western blot analysis

Total cellular protein was extracted using RIPA lysis buffer (P0013E; Beyotime) and the amount of protein was measured with a BCA Protein Assay Kit (P0011; Beyotime). Equal amounts of protein were then loaded and separated by SDS-PAGE, followed by transfer onto nitrocellulose (NC) membranes. After blocking with 5% non-fat milk for 1 h at room temperature, we incubated them with specific primary antibodies overnight at 4°C. The following day, the membranes were incubated with horseradish peroxidase (HRP)-conjugated secondary antibodies for 1 h at room temperature. Protein bands were visualized using an enhanced chemiluminescence (ECL) kit (Bio-Rad) and analyzed with Image Lab software (version 6.1). The primary antibodies are listed in Supplementary Table 1.

EdU Cell Proliferation Assay

We seeded cells into 6-well plates. After cell attachment, the cells were incubated with EdU working solution (ST067; Beyotime) for 2 h. Next, cells were fixed in 4% paraformaldehyde and permeabilized in 0.5% Triton X-100. Then we did fluorescent staining. Images were captured under a fluorescence microscope. Finally, the proportion of EdU-positive cells was calculated to evaluate the proliferative capacity of cells.

Cell Invasion Assay

Cell invasion ability was evaluated using Transwell chambers (FTW067; Beyotime). Prior to the assay, the upper surface of the membrane was pre-coated with Matrigel (BD Biosciences) to mimic the extracellular matrix. Cells from each group were resuspended in serum-free medium and seeded into the upper chambers, while medium supplemented with 10% FBS was added to the lower chambers to serve as a chemoattractant. After incubation for 48 h, non-invaded cells and the Matrigel on the upper surface were gently removed with a cotton swab. The invaded cells on the lower surface were fixed with 4% paraformaldehyde and stained with 0.1% crystal violet. The images of invaded cells was observed and captured in multiple randomly selected fields under a microscope.

Subcutaneous xenograft and syngeneic tumor models

All animal experiments were approved by the Animal Ethics Committee of Xi'an Jiaotong University for all animal experiments (Approval No. XJTUAE2026-2025), and the experiments were then carried out following the institution's rules for laboratory animal care and use.

Immunodeficient tumor models were established using 3-week-old male BALB/c nude mice, while immunocompetent tumor models were established using 4-week-old male C57BL/6 mice to generate subcutaneous tumor models. The former was used for human tumor xenografts, and the latter for syngeneic mouse tumor models. These animals were purchased from Laboratory Animal Center in Xi'an Jiaotong University.

Huh7 or Hepa1-6 cells with stable CHD2 knockdown (2.5×10^6 cells) were suspended in 100 μL PBS and subcutaneously injected into the right flank of mice. Each group contained five mice (n = 5). Mice were assigned to the control group or CHD2 knockdown group randomly.

Tumor growth was monitored every 3 days, and tumor length (L) and width (W) were measured using calipers. Tumor volume was calculated using the formula: $V = (L \times W^2) / 2$.

At the experimental endpoint, mice were euthanized according to ethical regulations. Tumors were excised, weighed, and measured, and subsequently used for immunohistochemical analysis.

Immunohistochemistry (IHC)

We fixed tumor tissues in 4% paraformaldehyde, then embedded them in paraffin and cut them into sections. Those sections were first deparaffinized and rehydrated. After that, we did antigen retrieval and blocked nonspecific binding sites.

Sections were then incubated with primary antibodies (antibody information is provided in Supplementary Table 1). Subsequently, the sections were incubated with appropriate secondary antibodies, followed by visualization using a 3,3'-diaminobenzidine (DAB) chromogen kit. Hematoxylin was applied for nuclear counterstaining.

The stained sections were observed with a light microscope, and images were taken from multiple randomly selected fields. The results were evaluated using a semi-quantitative scoring method based on staining intensity and the proportion of positive cells.

Chromatin Immunoprecipitation followed by quantitative PCR (ChIP-qPCR)

Cells were crosslinked at room temperature with formaldehyde to a final concentration of 1%, and the reaction was quenched by adding glycine. Cells were harvested and resuspended in SDS-containing ChIP lysis buffer, followed by lysis on ice. Chromatin was then sheared by sonication to obtain DNA fragments of appropriate size. After centrifugation, the supernatant was collected, and 1% of the lysate was saved as input control. The remaining samples were diluted with ChIP dilution buffer and incubated overnight at 4°C with 2 μg of specific antibody or normal IgG as a negative control.

The following day, Protein A/G magnetic beads were added to capture the immune complexes. Beads were sequentially washed with low-salt wash buffer, high-salt wash buffer, LiCl wash buffer, and TE buffer to remove nonspecific binding.

The immunoprecipitated chromatin complexes were then eluted, and crosslinks were reversed by incubation at 65°C overnight. Samples were subsequently treated with RNase A and proteinase K, and DNA was purified using a DNA purification kit. The purified DNA was finally subjected to quantitative PCR analysis.

Statistical analysis

All experiments were independently repeated at least three times. Data are presented as mean ± SD. Statistical analyses were performed using GraphPad Prism 8 software. Two-group comparisons were done with a two-tailed unpaired Student's t-test. Multiple group comparisons were done with one-way ANOVA followed by Tukey's post hoc test. A P value < 0.05 was considered statistically significant. Statistical significance is indicated as follows: * $P < 0.05$, ** $P < 0.01$, *** $P < 0.001$, and ns indicates no statistically significant difference.

Results

CHD2 is upregulated in HCC

We first evaluated CHD2 mRNA expression in the TCGA-LIHC cohort and observed that CHD2 was significantly upregulated in tumor tissues compared with non-paired normal tissues (Fig. 1A) and paired tumor–adjacent normal tissues (Fig. 1B). Consistent results were also obtained in the ICGC cohort (Fig. 1C).

We further analyzed RNA-seq datasets of HCC from GEO and found that CHD2 was upregulated in most datasets, although downregulated in a small subset of studies (Fig. 1F). In addition, protein expression from the CPTAC database also demonstrated increased CHD2 expression in HCC (Fig. 1D). IHC data from the HPA also revealed stronger CHD2 staining intensity in HCC tumor tissues (Fig. 1G). Moreover, we showed CHD2 expression across 33 cancer types in TCGA (Fig. 1E).

We also analyzed the expression of CHD family genes in HCC and found that CHD1, CHD2, CHD3, CHD4, CHD6, CHD7, and CHD8 were all upregulated in tumor tissues ($p < 0.05$) (Fig. S1A).

Furthermore, we also analyzed CHD2 expression in normal tissues using the GTEx database. It turned out that CHD2 levels were high in the lung, ovary, thyroid, epithelial cells, and fibroblasts, while it was relatively low in heart, brain, and liver tissues (Fig. S1C, S1D). We also assessed CHD2 expression across cancer cell lines in CCLE and found that it was highest in myeloma and lowest in adrenocortical carcinoma cell lines (Fig. S1E).

Finally, ROC curve analysis was used to analyze the diagnostic performance of CHD2 across pan-cancer types. CHD2 showed moderate diagnostic value in HCC with an AUC of 0.729 and exhibited good diagnostic performance in multiple cancer types (Fig. 1H and Fig. S1B).

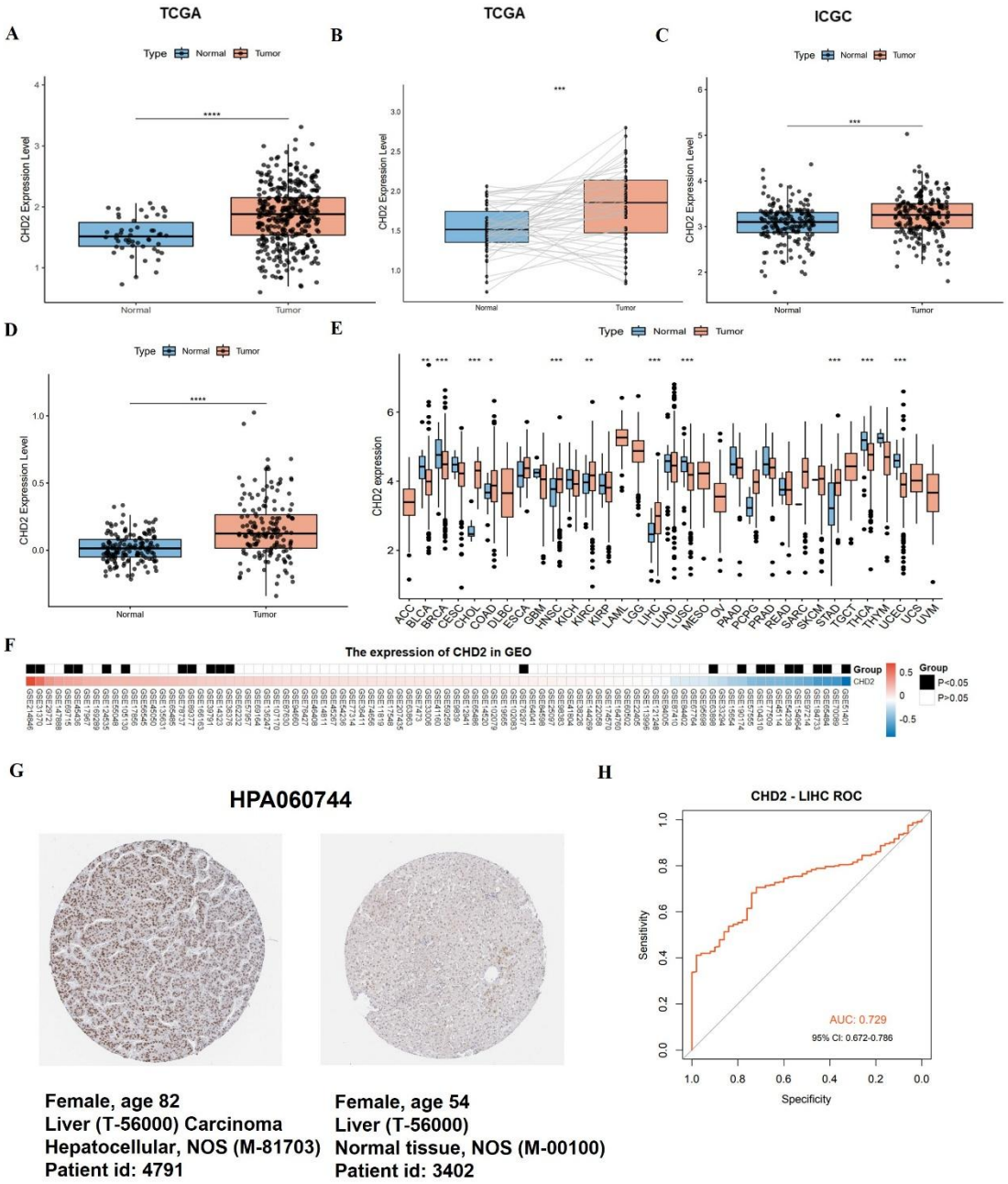


FIGURE 1 | CHD2 is upregulated in HCC across multiple datasets.(A, B) Expression of CHD2 in unpaired and paired samples from the TCGA-LIHC cohort.(C, F) Expression of CHD2 in the ICGC (LIRI-JP) dataset and 87 GEO liver cancer datasets.(D) Protein abundance of CHD2 in the CPTAC dataset.(E) Expression profile of CHD2 across 33 cancer types in TCGA.(G) Expression of CHD2 in the tumor and normal tissues.(H) ROC curve assessing the diagnostic ability of CHD2.(*p < 0.05, **p < 0.01, ***p < 0.001, ****p<0.0001)

CHD2 is associated with poor prognosis in HCC patients

We found that patients with high CHD2 expression exhibited worse OS, PFS, and DSS, as well as

a higher mortality risk score (Fig. 2A–F). We further visualized the differences in clinical characteristics between the CHD2-high and CHD2-low expression groups using a donut plot (Fig. 2G). In addition, we observed that CHD2 expression generally increased with advancing tumor stage (Fig. S2A). Compared to male patients, female patients had higher CHD2 expression. (Fig. S2B).

Based on the immune classification of cancer proposed by Thorsson et al[15], which stratifies tumors into six immune subtypes (C1–C6), we evaluated CHD2 expression across these immune categories. We found that CHD2 expression was higher in C1 and C3 subtypes (Fig. S2C).

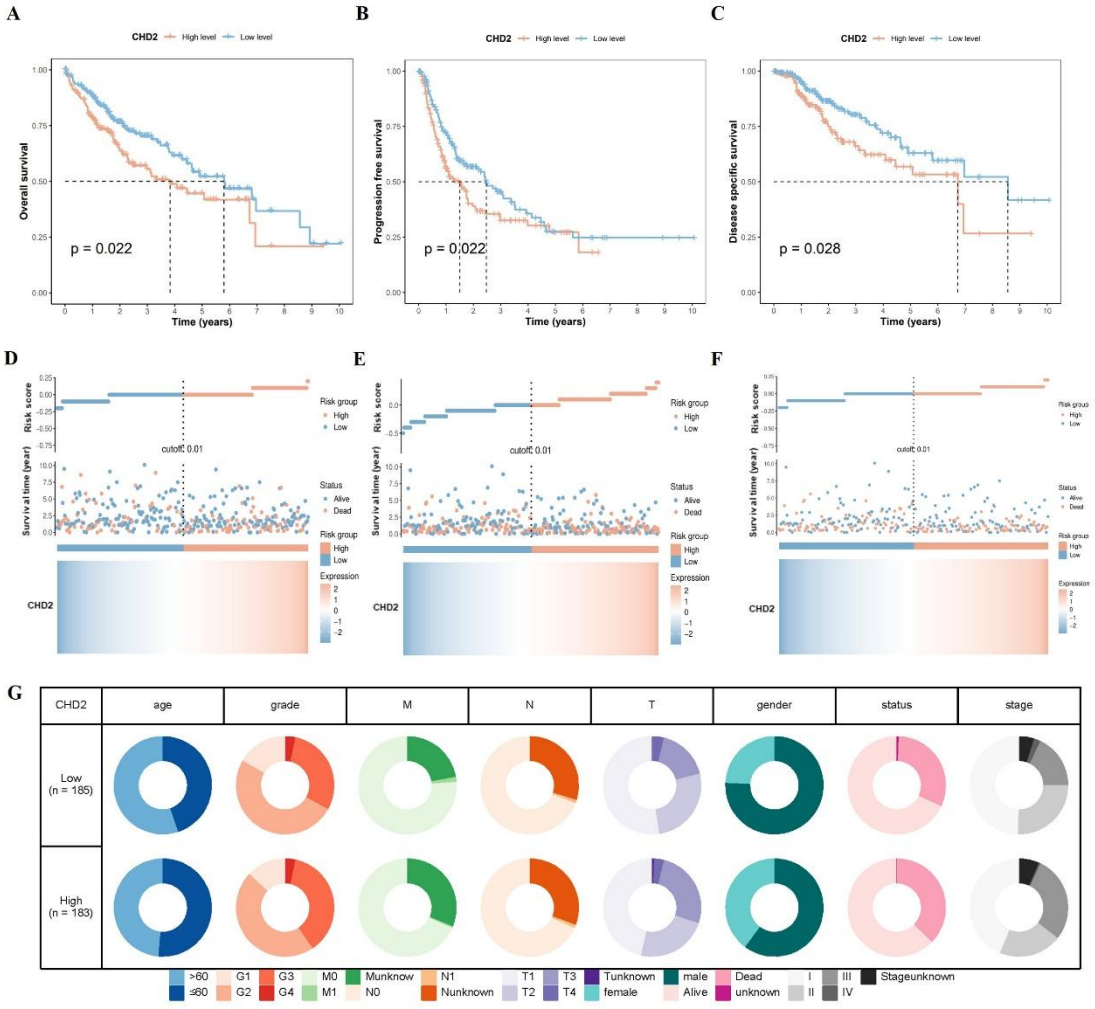


FIGURE 2 | (A–F) Kaplan–Meier survival curves and risk scores for OS, PFS, and DSS between CHD2-high and CHD2-low expression groups.(G) Clinical characteristic between CHD2-high and CHD2-low expression groups.

CHD2 is associated with an Immunosuppressive TME in HCC

First, we analyzed the levels of tumor immune infiltration based on the ESTIMATE algorithm.

We found that the ImmuneScore of the CHD2-low group was higher than that of the CHD2-high group (Fig. 3A), suggesting that high CHD2 expression may be associated with a less immune-enriched microenvironment. Then, we compared the differences in the infiltration of 22 types of immune cells between the CHD2-high and CHD2-low expression groups. The results showed higher infiltration levels of naïve B cells, resting memory $CD4^+$ T cells, and follicular helper T cells in the CHD2 high-expression group. Conversely, $CD8^+$ T cells, γδ T cells, activated NK cells, monocytes, and M2 macrophages were more enriched in the CHD2 low-expression group (Fig. 3B).

Next, we used multiple algorithms to evaluate the relationship between CHD2 expression and immune cell infiltration. CIBERSORT analysis revealed that CHD2 expression was positively correlated with naïve B cells, memory B cells, resting memory $CD4^+$ T cells, M1/M2 macrophages, activated mast cells, monocytes, neutrophils, plasma cells, and regulatory T cells, while it was negatively correlated with $CD8^+$ T cells, eosinophils, M0 macrophages, activated NK cells, and γδ T cells. TIMER analysis indicated that CHD2 expression showed a positive correlation with the infiltration of B cells, $CD4^+$ T cells, dendritic cells, macrophages, and neutrophils. The xCell algorithm showed that CHD2 expression showed a positive correlation with memory $CD4^+$ T cells, central memory T cells, mast cells, common lymphoid progenitors, and Tregs, while showing negative correlations with Th1/Th2 cells, plasmacytoid dendritic cells (pDC), endothelial cells, eosinophils, and NK cells. Results from MCP-counter, quanTIseq, and EPIC partially supported these conclusions ($p < 0.05$, Fig. 3C).

At the level of immune-related genes, CHD2 expression was modestly associated with various chemokines and their receptors. CHD2 showed strong moderate positive correlations with CCR4 ($r = 0.40$), IL6R ($r = 0.39$), and XCR1 ($r = 0.34$), while displaying negative correlations with CCL3 ($r = -0.24$), CCL15 ($r = -0.23$), and CXCL17 ($r = -0.18$) (Fig. 3D). Furthermore, the expression of CD274 (PD-L1) was positively correlated with CHD2 ($r = 0.21$). Analysis based on the TISIDB database further examined differences in immunostimulators, immunoinhibitors, chemokines, and human leukocyte antigens (HLA) between the CHD2-high and CHD2-low expression groups (Fig. S3A). Consistent with previous findings, patients with high CHD2 levels showed a significant positive with CD274 expression ($p < 0.001$).

The cancer-immunity cycle consists of several key steps. Correlation analysis revealed that CHD2 expression showed a positive correlation with Step 4 (Th17 cell recruitment), but negatively correlated with steps such as priming and activation, dendritic cell recruitment, macrophage recruitment, eosinophil recruitment, Th2 cell recruitment, infiltration of immune cells into tumors, and the killing of cancer cells (Fig. 3E).

Furthermore, we analyzed the correlation between CHD2 expression and 18 immune features. The results demonstrated that CHD2 expression was positively correlated with TGF-β response, cell proliferation, TCR richness, and TCR Shannon index, with the correlation to TGF-β response

being the most significant (Fig. 3F).

Additionally, we investigated the correlation between CHD2 expression and 68 immune characteristic signatures. The results showed that CHD2 expression had the strongest positive correlation with the $CD103^{+}/CD103^{-}$ ratio, and the most significant negative correlation with the CSR Activated feature ($p < 0.05$, Fig. 3G).

Finally, the TCGA-LIHC cohort was divided into four subgroups (Q1–Q4) based on CHD2 expression levels. We systematically analyzed the mRNA expression, methylation levels, and the frequency of amplification and deletion of immunomodulators across the different subgroups (Fig. S3B), and explored their relationships with immune responses and genomic characteristics (Fig. S3C).

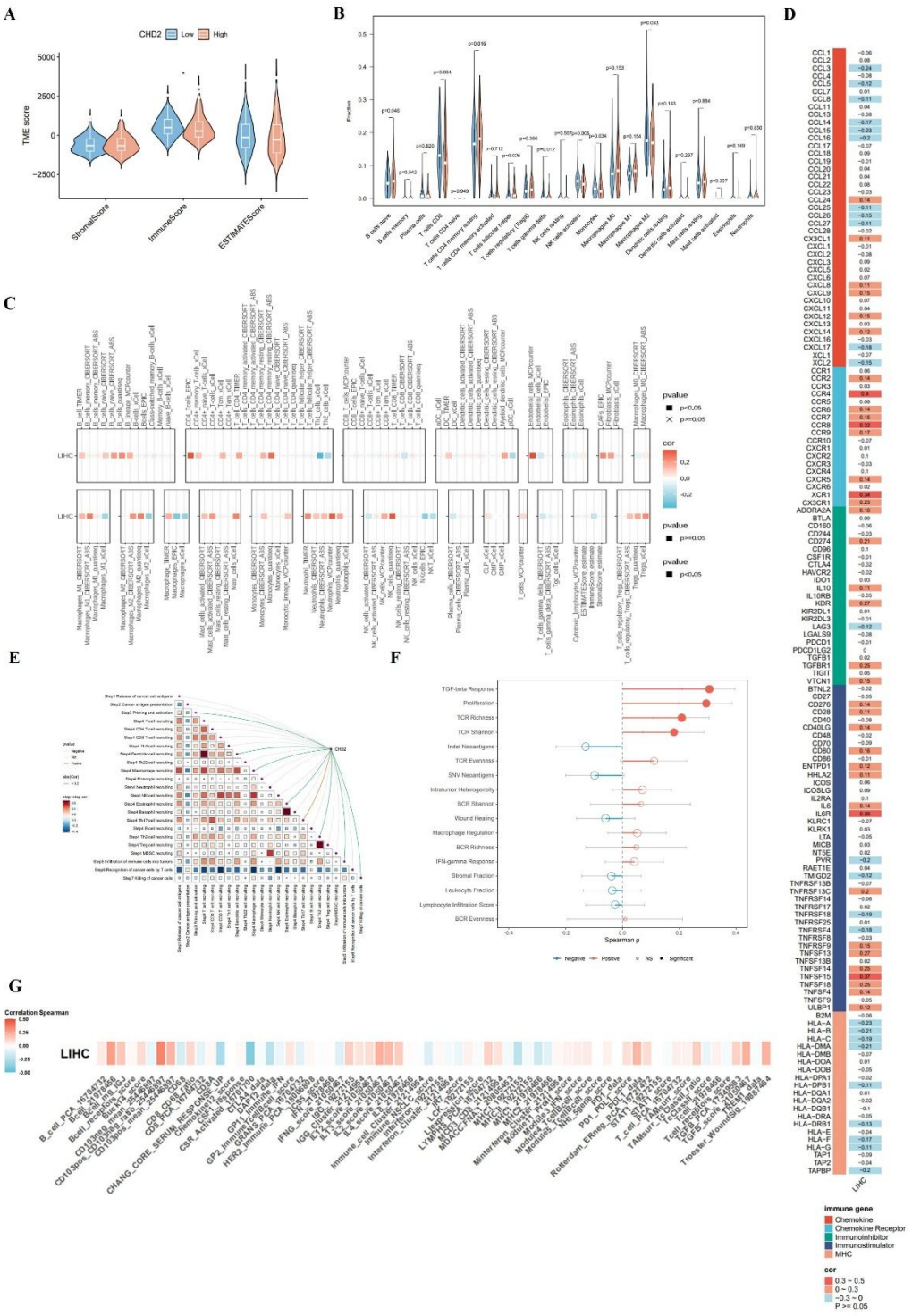


FIGURE 3 | Correlation between CHD2 expression and immune infiltration in TCGA-LIHC.(A) Tumor TME scores in CHD2-high and CHD2-low expression groups.(B) Differences in infiltration levels of 22 immune cell types between CHD2 -high(red) and CHD2-low (blue) expression groups.(C) Correlation between CHD2 expression and immune cell infiltration estimated by multiple algorithms.(D) Correlation analysis between CHD2 expression and immune-related molecules, including chemokines, chemokine receptors, immunoinhibitors, immunostimulators, and MHC molecules.(E–G) Correlation analyses of CHD2 expression with the cancer immunity cycle, 18 immune features, and 68 immune signature scores.

CHD2-Positive Malignant Cells Enhance TGF-β superfamily Signaling and Immunosuppressive Features in HCC

We performed clustering and annotation on scRNA-seq data, identifying a total of 12 cell subpopulations. These include mast cells, regulatory T cells, $CD8^+$ T cells, B cells, monocytes/macrophages, dendritic cells, proliferating T cells, fibroblasts, endothelial cells, epithelial cells, and malignant cells (Fig. 4A). Visualization of CHD2 expression on the UMAP plot revealed that it is enriched in malignant cells (Fig. 4B, D). After categorizing cells into CHD2-positive and CHD2-negative groups, the malignant cells exhibited the highest proportion in the positive group (35.4%), suggesting that CHD2 is highly expressed in tumor cells (Fig. 4C). In addition, Fig.5A, D and Fig.S4A show diagrams of communication patterns for individual cell subpopulations.

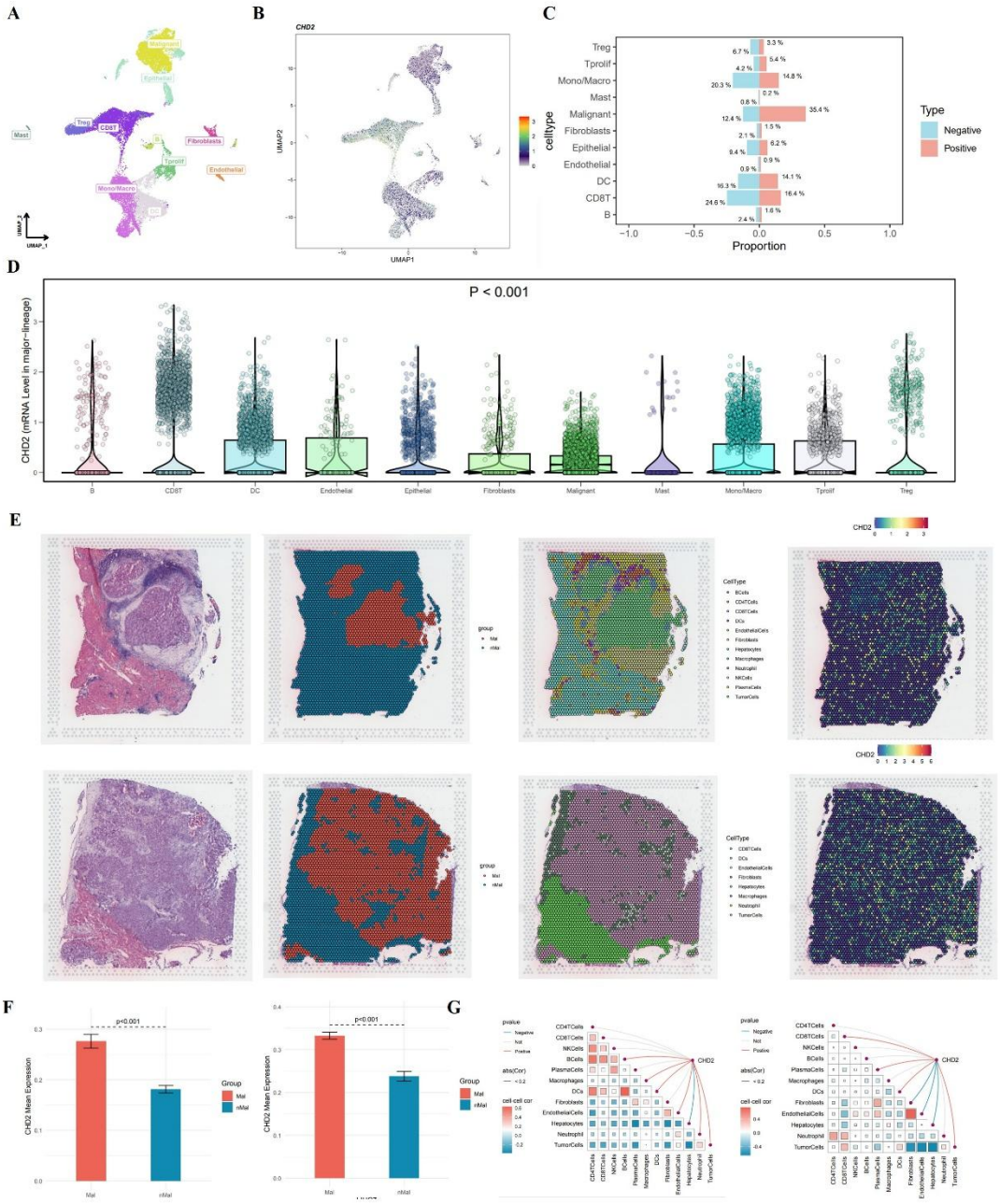


FIGURE 4 | CHD2 is highly expressed in tumor cells in single-cell and spatial transcriptomic datasets.(A) UMAP plot showing major cell types in the GSE166635 dataset.(B) UMAP plot showing the distribution of CHD2 expression.(C) Proportional differences of CHD2-positive and CHD2-negative cells across cell types.(D) Bar plot showing CHD2 expression across different cell clusters.(E) Spatial transcriptomic section annotation, including region segmentation, cell type annotation, and CHD2 expression distribution.(F) Differential expression of CHD2 between malignant and non-malignant regions.(G) Correlation analysis between CHD2 expression and various cell types at the spatial TME level.

Cell-cell communication analysis suggested that CHD2-positive malignant cells exhibited enhanced activity in both outgoing and incoming signaling (Fig. 5B–C). Notably, these cells were enriched in signaling pathways such as BMP, Activin, and GDF, all of which belong to the TGF-β

superfamily. Regarding incoming signals, CHD2-positive malignant cells showed increased sensitivity to Periostin and IL1 signaling. These results suggest that CHD2-positive malignant cells act both as senders, strengthening their regulation of surrounding cells, and as receivers, becoming more sensitive to microenvironment. Moreover, they may modulate the immunosuppressive TME through pathways related to the TGF-β superfamily.

The expression and spatial distribution of CHD2 were further validated in two spatial transcriptomics samples. The results showed that CHD2 was overexpressed in malignant regions (Fig. 4E–F) and positively correlated with DCs and tumor cells, while showing a negative correlation with hepatocytes (Fig. 4G).

Furthermore, we analyzed the relationship between CHD2 and the TGF-β/SMAD pathway at both scRNA-seq and spatial transcriptomic levels. We found that CHD2 co-localized and showed a strong positive correlation with key molecules of the TGF-β/SMAD pathway, including TGF-β 1/3 and SMAD2/3 (Fig. 5E, F; Fig. S4B, C). Additionally, we calculated the TGF-β/SMAD pathway score at the spatial level using VAM enrichment scores (Fig. 5G).

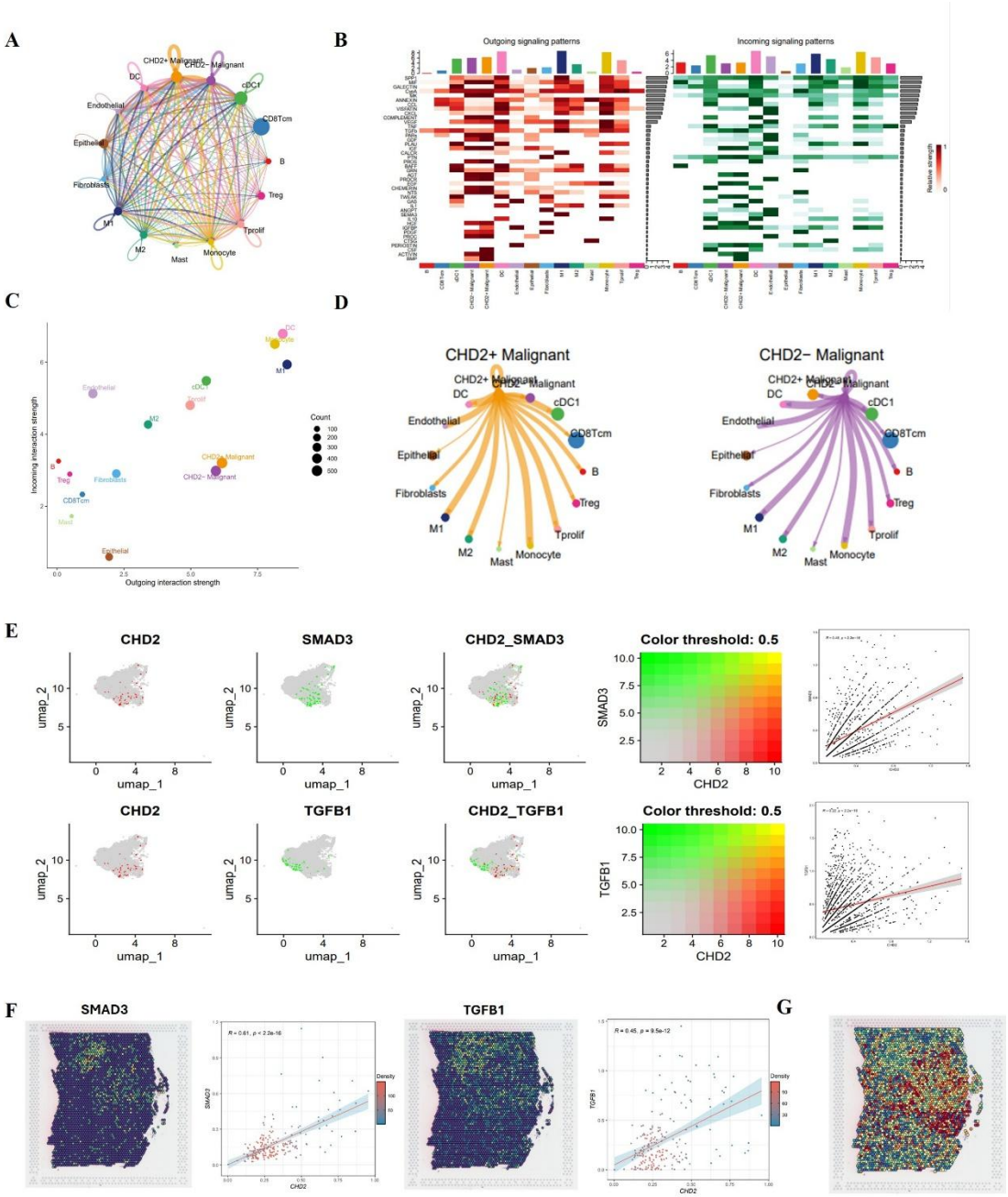


FIGURE 5 | Cell–cell communication and pathway analyses at the single-cell level.(A) Cell–cell communication network among different cell subpopulations.(B, C) Major incoming and outgoing signaling patterns across cell populations.(D) Interaction strength analysis between CHD2^{+} malignant cells, CHD2^{-} malignant cells, and other cell subpopulations.(E) Co-localization and correlation analyses of SMAD3 and TGF-β1 with CHD2 using the scRNA-seq dataset.(F) Spatial expression of SMAD3 and TGF-β1 and pseudo-bulk correlation analysis with CHD2.(G) VAM enrichment scores of the TGF-β/SMAD pathway in spatial transcriptomics.

The Role of CHD2 in Methylation Modification and Genomic Stability

We first analyzed the association of CHD2 expression and RNA methylation regulators related to m1A, m5C, and m6A modifications across pan-cancers (Fig. 6A). Further methylation analysis of CpG islands within the CHD2 gene revealed varying degrees of methylation across 18 specific sites (Fig. 6B), suggesting that CHD2 may be regulated by multi-layered methylation modification.

At the genomic level, we examined the CNVs of CHD2. Significant differences in CHD2 expression were observed among different CNV groups, with the amplification group exhibiting the highest expression levels (Fig. 6C, $p < 0.01$). Moreover, the infiltration levels of six types of immune cells varied across different CHD2 CNV states (Fig. 6E), indicating that CNVs may influence the TME by modulating immune infiltration.

Furthermore, we evaluated the relationship between CHD2 and indicators of genomic stability. Loss of heterozygosity (LOH) is a chromosomal event that can lead to the loss of an entire gene and its adjacent regions. Our analysis showed that CHD2 expression was negatively correlated with the LOH score in HCC samples (Fig. 6D), suggesting that CHD2 may play a part in maintaining genomic stability.

Finally, we explored the association between CHD2 expression levels and key oncogenes as well as canonical signaling pathways. The results indicated that patients with high CHD2 expression in HCC exhibited higher mutation frequencies in genes such as TP53 and RPS6KA3 (Fig. 6F–G). This suggests that CHD2 may be involved in regulating genomic instability and tumor-driving events.

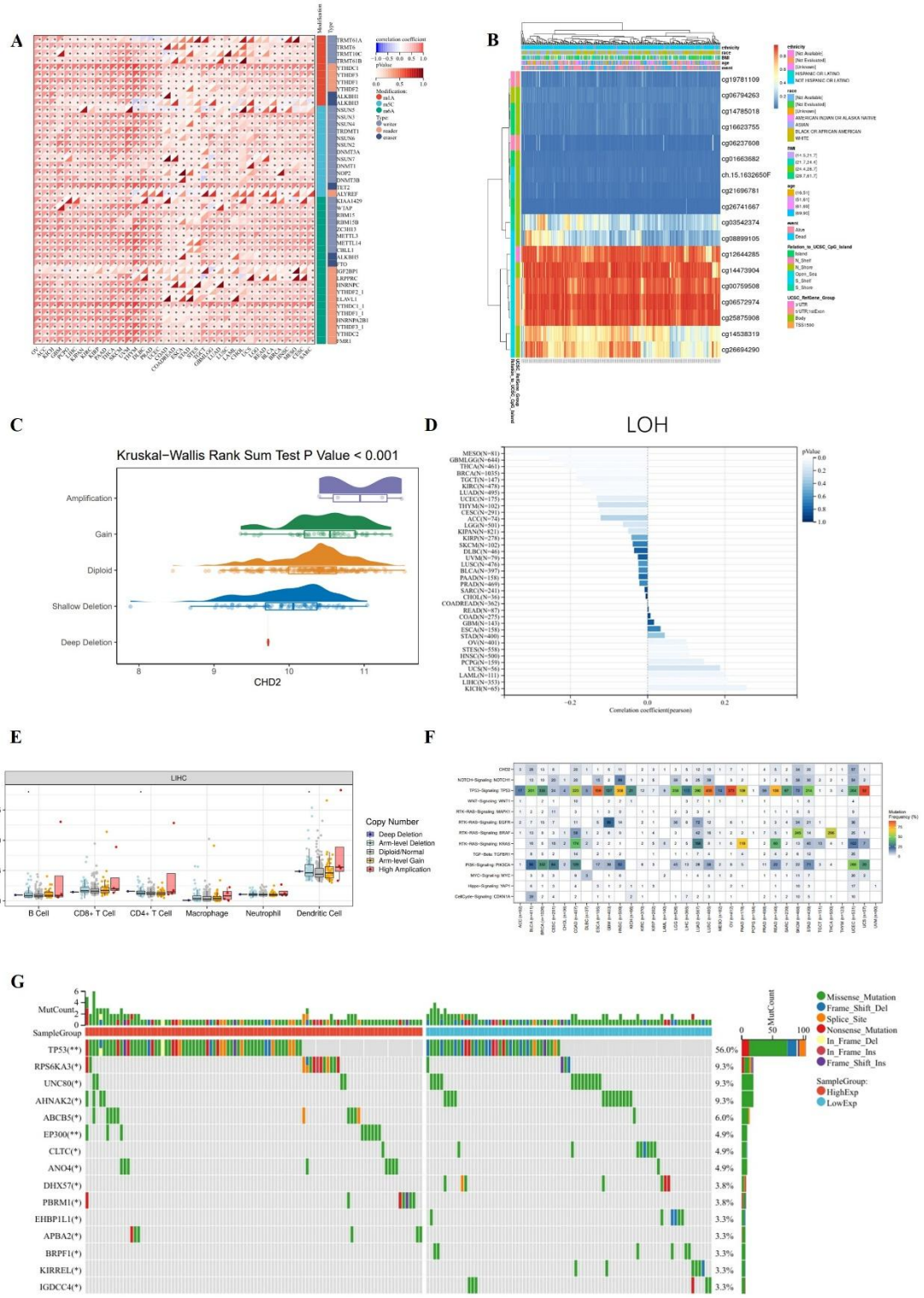


FIGURE 6 | CHD2 methylation and genomic instability analyses.(A) CHD2 methylation levels across multiple cancer types.(B) Methylation levels of individual CpG sites within CHD2.(C) CHD2 expression across different CNV types.(D) Correlation between loss of heterozygosity (LOH) scores and CHD2 expression across cancers.(E) Association between CNV and immune infiltration levels.(F) Correlation between CHD2 and mutations in classical oncogenic signaling pathways.(G) Top 15 mutated genes in CHD2-high and CHD2-low expression groups.

Potential Drug screening for CHD2

To explore potential therapeutic intervention strategies for CHD2, we utilized four types of chemotherapy-related gene sets to evaluate the correlation between CHD2 and drug response (Fig. S5A). Further analysis through the cMAP database identified MK-886 as a potential small-molecule candidate targeting CHD2 (Fig. S5B).

In silico knockout analysis of CHD2

To investigate the potential molecular mechanisms and regulatory effects associated with CHD2 depletion, we performed in silico knockout analysis using the scTenifoldKnk algorithm in the HCC single-cell dataset GSE146115. Following knockout of CHD2, COX4I1 was identified as the most significantly perturbed gene (Fig. 7A, B).

KEGG pathway enrichment analysis of the perturbed genes revealed significant enrichment in oxidative phosphorylation, mineral absorption, glycolysis/gluconeogenesis, chemical carcinogenesis–reactive oxygen species, and amino acid biosynthesis pathways (Fig. 7C). Gene Ontology (GO) analysis further demonstrated that mitochondrial electron transport chain activity and oxidation–reduction-related biological processes were markedly affected (Fig. 7D). These findings suggest that CHD2 depletion may substantially impair mitochondrial function, energy metabolism, and oxidative stress-related pathways.

To evaluate the functional dependency of CHD2 across multiple cancer types, we analyzed CERES scores derived from genome-wide CRISPR-Cas9 screening data in the DepMap database. Overall, CHD2 exhibited CERES scores below zero in most cancer cell lines, indicating a broad functional dependency (Fig. 7E). Among HCC cell lines, SNU398 showed the strongest dependency on CHD2, whereas SNU182 exhibited the weakest dependency.

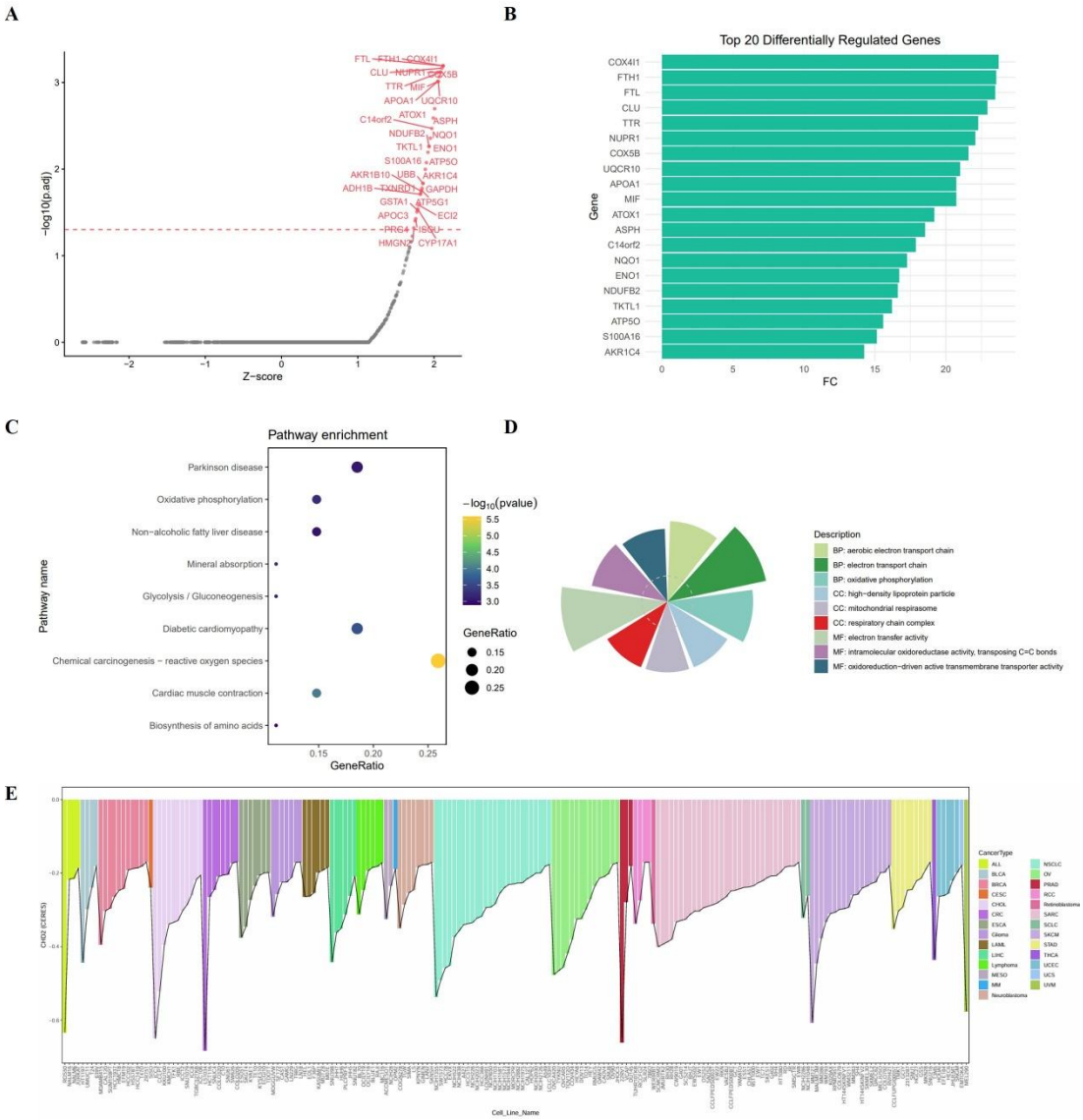


FIGURE 7 | In silico knockout of CHD2 and downstream analyses.(A) In silico knockout of CHD2 using scTenifoldKnk.(B) Top 20 differentially regulated genes following CHD2 virtual knockout.(C, D) GO and KEGG enrichment analyses of downstream regulated genes.(E) Distribution of CHD2 CERES scores across pan-cancer cells from genome-wide CRISPR-Cas9 screening in the DepMap database.

Functional enrichment analysis and downstream pathway identification of CHD2

Differential expression analysis was used based on CHD2 expression in patients, and DEGs were found (p.adjust < 0.05, |logFC| > 0.3) (Fig. 8A). GO analysis found that these genes were mainly involved in cell adhesion, axonogenesis, and extracellular matrix-related biological processes (Fig. 8B).

KEGG pathway enrichment and GSEA analyses demonstrated that high CHD2 expression was

significantly associated with the TGF-β, Wnt/β-catenin, and PI3K-Akt signaling pathways (Fig. 8C, D).

We further analyzed the correlations between CHD2 expression and 14 tumor functional states (Fig. 8E). The results showed that CHD2 expression was positively correlated with stemness ($r = 0.38$), angiogenesis ($r = 0.28$), differentiation ($r = 0.37$), apoptosis ($r = 0.24$), DNA damage ($r = 0.23$), EMT ($r = 0.19$), hypoxia ($r = 0.15$), inflammation ($r = 0.16$), metastasis ($r = 0.25$), proliferation ($r = 0.26$), and quiescence ($r = 0.25$).

Finally, PPI networks associated with CHD2 were constructed using the ComPPI and GeneMANIA databases, systematically illustrating its potential molecular interactions and downstream regulatory networks (Fig. 8F, G).

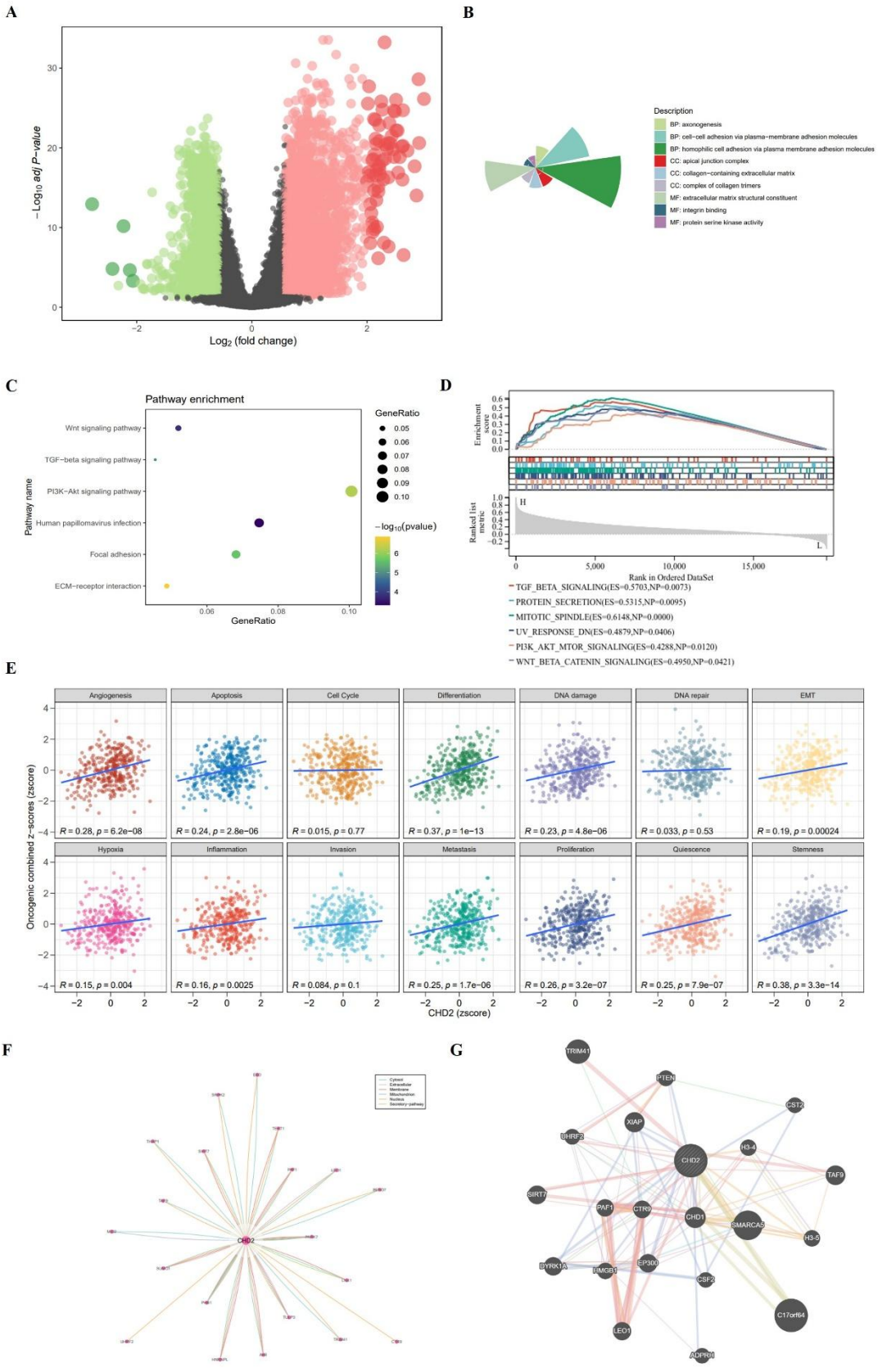


FIGURE 8 | Downstream pathway analyses, functional enrichment, and PPI network construction.(A) Differentially expressed genes between CHD2-high and CHD2-low expression groups in HCC

patients.(B–D) GO, KEGG, and GSEA enrichment analyses of DEGs.(E) Correlation analysis between CHD2 expression and tumor functional scores in HCC.(F, G) Construction of CHD2-related PPI networks using ComPPI and GeneMANIA.

CHD2 is a target gene of HIF1-α and is regulated by hypoxia

To investigate the upstream regulatory mechanism of CHD2, we screened potential transcription factors of CHD2 using the hTFtarget, ChEA, and GTRD databases. Intersection analysis identified 30 potential transcription factors, including HIF1-α (Fig. 9A). In addition, overlap analysis between HIF1-α ChIP-seq targets and differentially expressed genes from hypoxia-related RNA-seq datasets identified CHD2 as a potential target gene of HIF1-α (Fig. 9B).

RNA-seq analysis under hypoxia demonstrated that CHD2 expression was significantly elevated in HepG2 and Hep3B cells compared with normoxic controls, and its expression gradually increased with prolonged hypoxia exposure (Fig. 9C; Fig. S6A, B). Furthermore, CHD2 expression was positively correlated with HIF1-α expression in both the TCGA-LIHC cohort (Fig. 9D) and the GSE41666 dataset (Fig. S6C). Similar findings were observed in single-cell and spatial transcriptomic analyses (Fig. S6F, J).

To further assess the association between CHD2 and hypoxia, we calculated hypoxia scores and found that high CHD2 expression was accompanied by significantly increased Winter hypoxia score (Fig. 9E). Correlation analyses in the GSE41666 dataset further showed that CHD2 expression positively correlated with hypoxia-related gene signatures from the GO and Reactome databases (Fig. S6D, E). In addition, the expression patterns of HIF1-α and HIF/hypoxia pathway activity were visualized in single-cell and spatial transcriptomic datasets (Fig. S6G–I).

Compared with the normal liver cell line THLE-2, CHD2 expression was markedly elevated in HCC cell lines. Huh7 and HCCLM3 cells were therefore selected for subsequent experiments (Fig. 9F). Overexpression of HIF1-α in Huh7 and HCCLM3 cells significantly increased CHD2 mRNA and protein expression levels (Fig. 9G, H). Moreover, CHD2 expression was markedly upregulated under hypoxia conditions, whereas HIF1-α knockdown reduced CHD2 expression at both the mRNA and protein levels (Fig. 9I, J).

To determine whether CHD2 is a direct transcriptional target of HIF1-α, ChIP assays were performed. Analysis of the 2,000 bp upstream region of the CHD2 promoter identified putative HRE binding sites. ChIP assays were subsequently conducted using anti-HIF1-α, anti-HIF1-β, and IgG antibodies, followed by PCR analysis of the immunoprecipitated DNA fragments. The results demonstrated that HIF1-α directly binds to the CHD2 promoter region in both Huh7 and HCCLM3 cells (Fig. 9K).

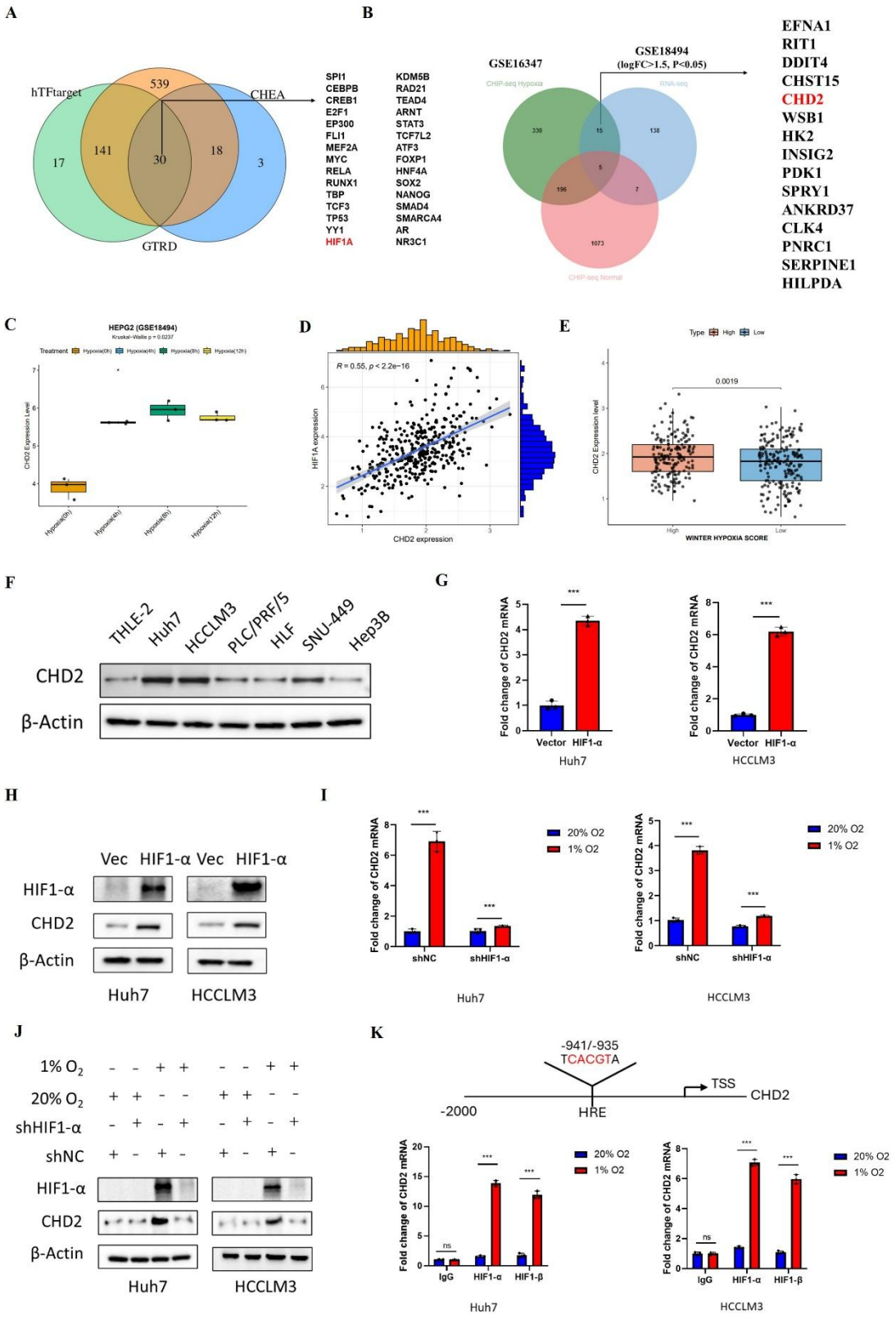


FIGURE 9 | CHD2 is a downstream target of HIF1-α and is regulated by hypoxia.(A) Identification of potential transcription factors regulating CHD2 using hTFtarget, ChEA, and GTRD databases.(B) Integrated ChIP-seq and RNA-seq analysis identifying hypoxia-upregulated genes and HIF1-α downstream targets.(C) Upregulation of CHD2 under hypoxia conditions. (D) Correlation between

CHD2 and HIF1-α expression in TCGA. (E) Differences in hypoxia-related scores between CHD2-high and CHD2-low expression groups. (F) Protein expression of CHD2 in HCC cell lines by western blot.(G, H) CHD2 mRNA and protein expression after HIF1-α overexpression by RT-qPCR and western blot.(I, J) CHD2 mRNA and protein expression after HIF1-α knockdown under normoxic and hypoxia conditions by RT-qPCR and western blot.(K) ChIP-qPCR assay performed in Huh7 and HCCLM3 cells exposed to 20% or 1% oxygen for 12 h.(***$p < 0.001$)

CHD2 knockdown suppresses proliferation, invasion, and EMT in vitro

To investigate the biological role of CHD2 in vitro, CHD2 was silenced in Huh7 and HCCLM3 cell lines. Western blot analysis demonstrated that CHD2 knockdown significantly increased the expression of the pro-apoptotic proteins BAX and cleaved caspase-3, indicating enhanced apoptosis. In contrast, the expression levels of CDK4 and Cyclin D1 were decreased, suggesting inhibition of cell cycle progression (Fig. 10A). EdU incorporation assays further showed that CHD2 knockdown significantly impaired the proliferation of HCC cells, as reflected by a reduced number of EdU-positive cells (Fig. 10B).

In addition, western blot analysis revealed that CHD2 knockdown increased the expression of the epithelial marker E-cadherin while decreasing the expression of the mesenchymal marker Vimentin, indicating suppression of the EMT process (Fig. 10C). Transwell assays further demonstrated that CHD2 knockdown significantly inhibited the invasion of HCC cells (Fig. 10D).

These findings indicate that CHD2 knockdown suppresses the malignant phenotypes of HCC cells by promoting apoptosis and inhibiting proliferation, invasion, and EMT progression.

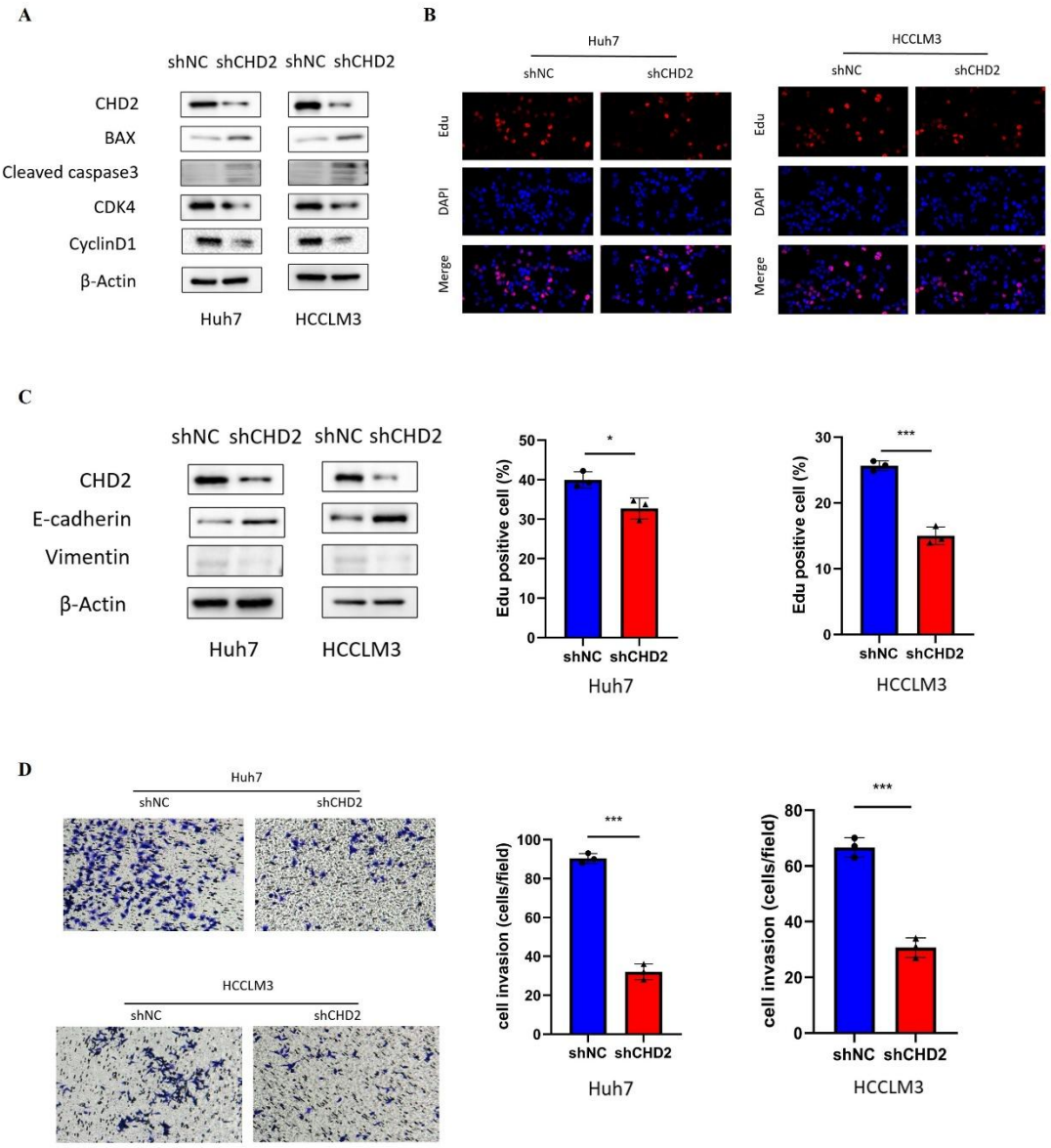


FIGURE 10 | Effects of CHD2 knockdown on HCC in vitro.(A) Western blot of BAX, cleaved caspase-3, CDK4, and Cyclin D1 expression after CHD2 knockdown in Huh7 and HCCLM3 cells by western blot.(B) EdU incorporation assay after CHD2 knockdown in Huh7 and HCCLM3 cells.(C) Western blot of EMT-related proteins E-cadherin and Vimentin after CHD2 knockdown in Huh7 and HCCLM3 cells.(D) Transwell assay showing decreased invasion ability after CHD2 knockdown in Huh7 and HCCLM3 cells.(*$p < 0.05$, ***$p < 0.001$).

CHD2 knockdown suppresses tumor growth and EMT in vivo

To evaluate the effects of CHD2 on HCC growth in vivo, a subcutaneous xenograft mouse model was established by injecting CHD2 knockdown Huh7 cells into BALB/c nude mice (Fig. 11A). Compared with the control group, CHD2 knockdown markedly suppressed tumor growth, resulting in significantly reduced tumor volume and tumor weight (Fig. 11B, C).

Immunohistochemistry further demonstrated that CHD2 knockdown increased the expression of the epithelial marker E-cadherin, while decreasing the expression of Ki-67 and Vimentin (Fig. 11D).

These results suggest that CHD2 knockdown significantly inhibits HCC growth in vivo and may exert its antitumor effects through regulating cell proliferation and EMT.

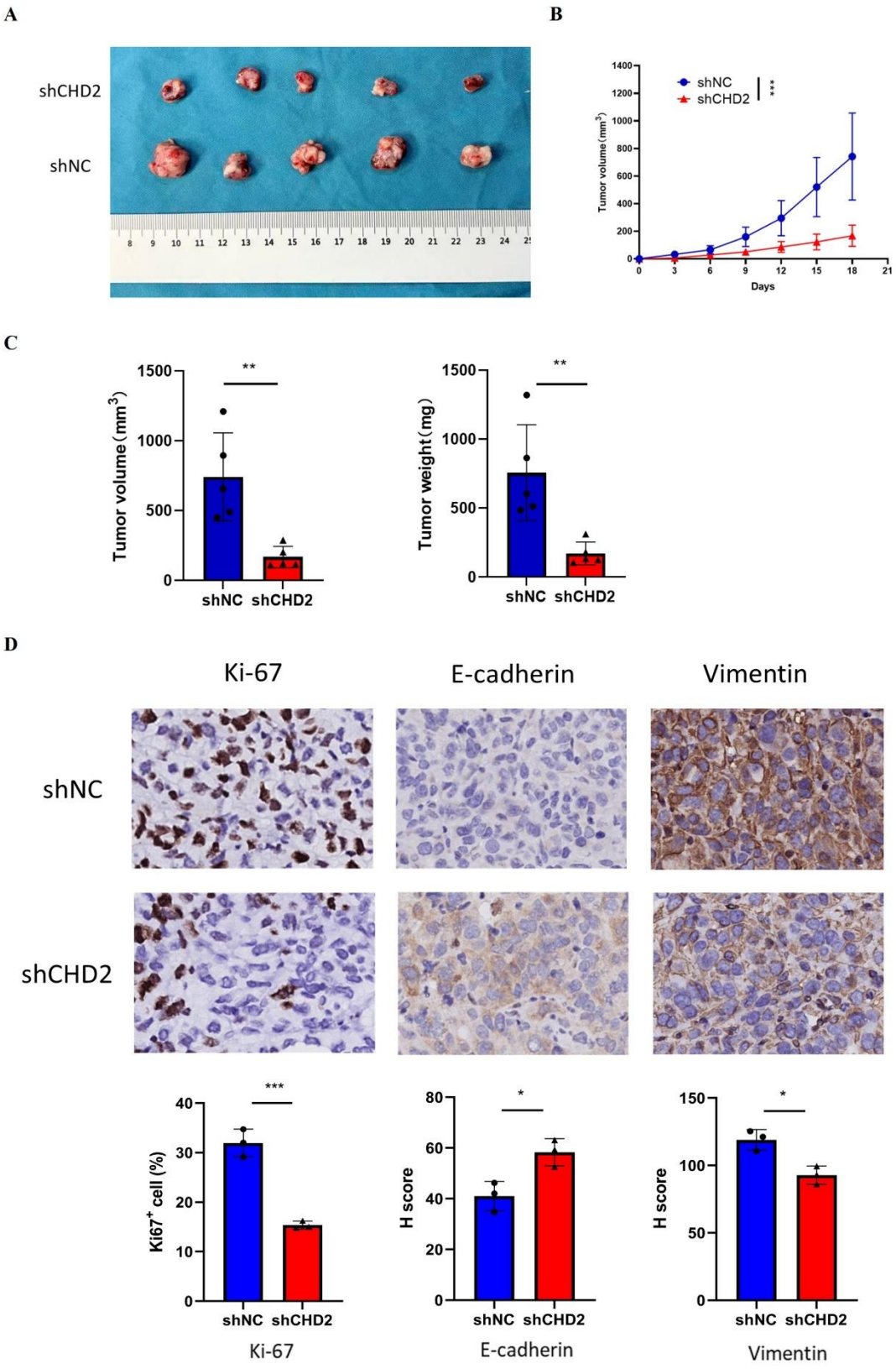


FIGURE 11 | Effects of CHD2 knockdown in vivo.(A) Subcutaneous xenograft model established by inoculating CHD2-knockdown Huh7 cells into nude mice.(B) Tumor growth curves measured over

time.(C) Statistical analysis of tumor volume and tumor weight at endpoint.(D) IHC of E-cadherin, Ki-67, and Vimentin.(*p < 0.05, **p < 0.01, ***p < 0.001)

CHD2 promotes HCC progression through the TGF-β/Smad signaling pathway

To investigate the molecular mechanism by which CHD2 promotes hepatocellular carcinoma progression, we integrated the results from scRNA-seq and spatial transcriptomic analyses. We found that CHD2 expression was positively correlated with the TGF-β/Smad signaling pathway, and pathway enrichment analyses also indicated activation of this pathway. Therefore, we hypothesized that CHD2 may promote HCC progression through regulation of the TGF-β/Smad signaling pathway.

Western blot analysis demonstrated that knockdown of CHD2 reduced the expression levels of TGF-β1/3 and phosphorylated Smad2/3 (p-Smad2/3) (Fig. 12A). In contrast, CHD2 overexpression significantly increased p-Smad2/3 expression, whereas this effect was markedly attenuated by treatment with the TGF-β receptor I inhibitor Vactosertib (Fig. 12B).

Functional assays further demonstrated that CHD2 overexpression enhanced cell proliferation, EMT, and invasion, while Vactosertib treatment significantly reversed these effects (Fig. 12C–E).

These findings indicate that CHD2 promotes the malignant phenotypes of HCC cells through activation of the TGF-β/Smad signaling pathway.

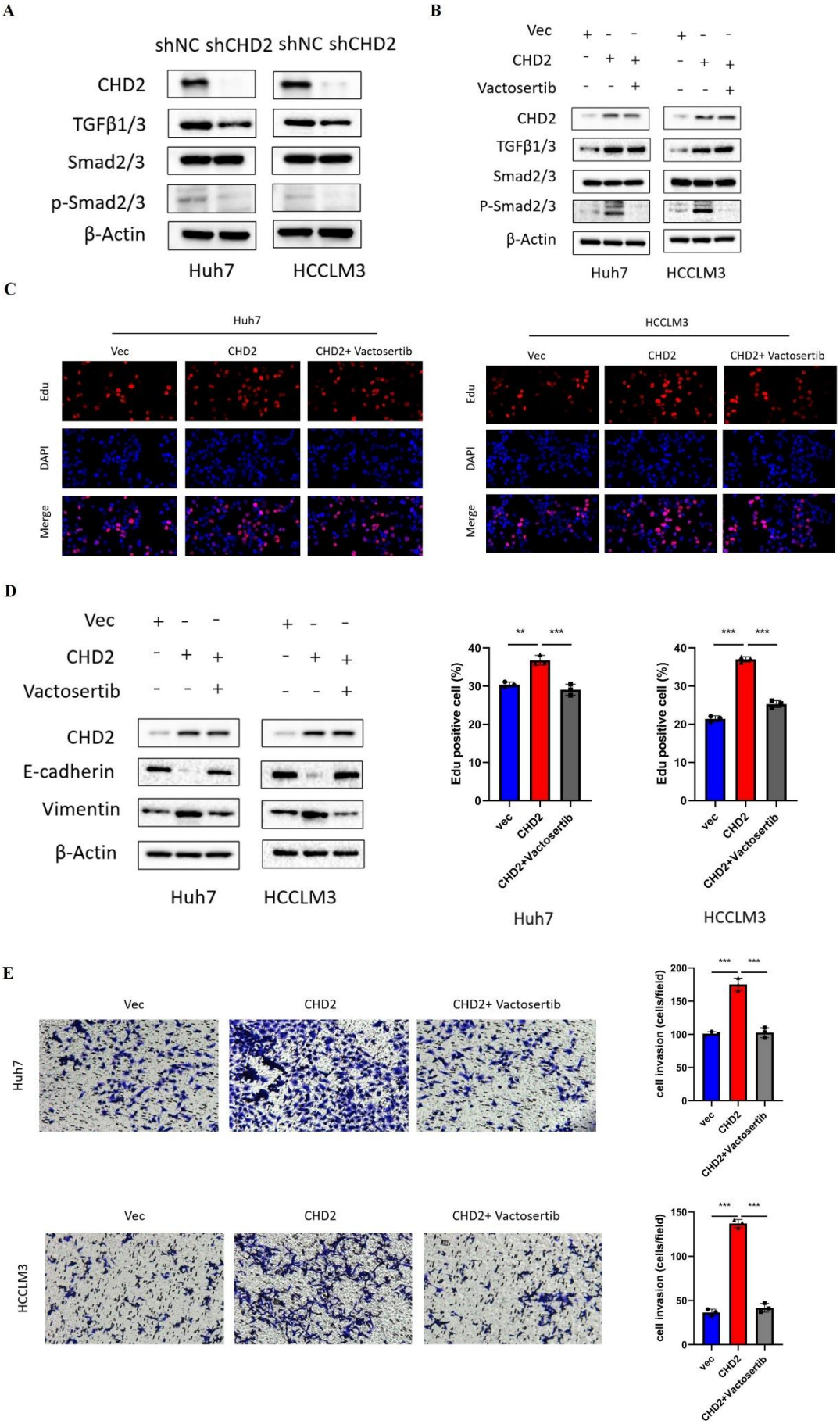

A
shNC shCHD2 shNC shCHD2
CHD2
TGFβ1/3
Smad2/3
p-Smad2/3
β-Actin
Huh7
HCCLM3
B
Vec
CHD2
Vactosertib
CHD2
TGFβ1/3
Smad2/3
P-Smad2/3
β-Actin
Huh7
HCCLM3
C
Huh7
HCCLM3
Vec
CHD2
CHD2+ Vactosertib
Edu
DAPI
Merge
D
Vec
CHD2
Vactosertib
CHD2
E-cadherin
Vimentin
β-Actin
Huh7
HCCLM3
Edu positive cell (%)
vec
CHD2
CHD2+Vactosertib
Huh7
HCCLM3
E
Huh7
HCCLM3
Vec
CHD2
CHD2+ Vactosertib
cell invasion (cells/field)
vec
CHD2
CHD2+Vactosertib

FIGURE 12 | CHD2 regulates HCC through the TGF-β/Smad pathway.(A) Western blot of TGF-β1/3 and p-Smad2/3 after CHD2 knockdown.(B) CHD2 overexpression increased p-Smad2/3 levels, which were reversed by Vactosertib by western blot.(C–E) Functional assays showing the effects of CHD2 overexpression on proliferation, EMT, and invasion, as well as the rescue effects of Vactosertib.(**$p < 0.01$, ***$p < 0.001$.)

CHD2 participates in the regulation of the TME

Based on previous bioinformatics analyses, CHD2 was suggested to be involved in the regulation of an immunosuppressive TME. To further validate this hypothesis, both in vitro and in vivo experiments were performed.

In vitro experiments showed that knockdown of CHD2 significantly reduced the expression of PD-L1 (Fig. 13A). Conversely, CHD2 overexpression increased PD-L1 expression, whereas this effect was reversed by Vactosertib treatment (Fig. 13B).

For in vivo experiments, a subcutaneous xenograft mouse model was established by injecting Hepa1-6 cells into C57BL/6 mice. The results demonstrated that CHD2 knockdown markedly suppressed tumor growth, resulting in reduced tumor volume and tumor weight (Fig. 13C–E).

IHC further revealed that CHD2 knockdown decreased PD-L1 expression while significantly increasing the expression of CD8 and GZMB (Fig. 13F), indicating a partial recovery of antitumor immune activity and a remission of the immunosuppressive state.

These findings suggest that CHD2 may promote immune evasion and HCC progression by activating the TGF-β/Smad pathway and upregulating PD-L1 expression.

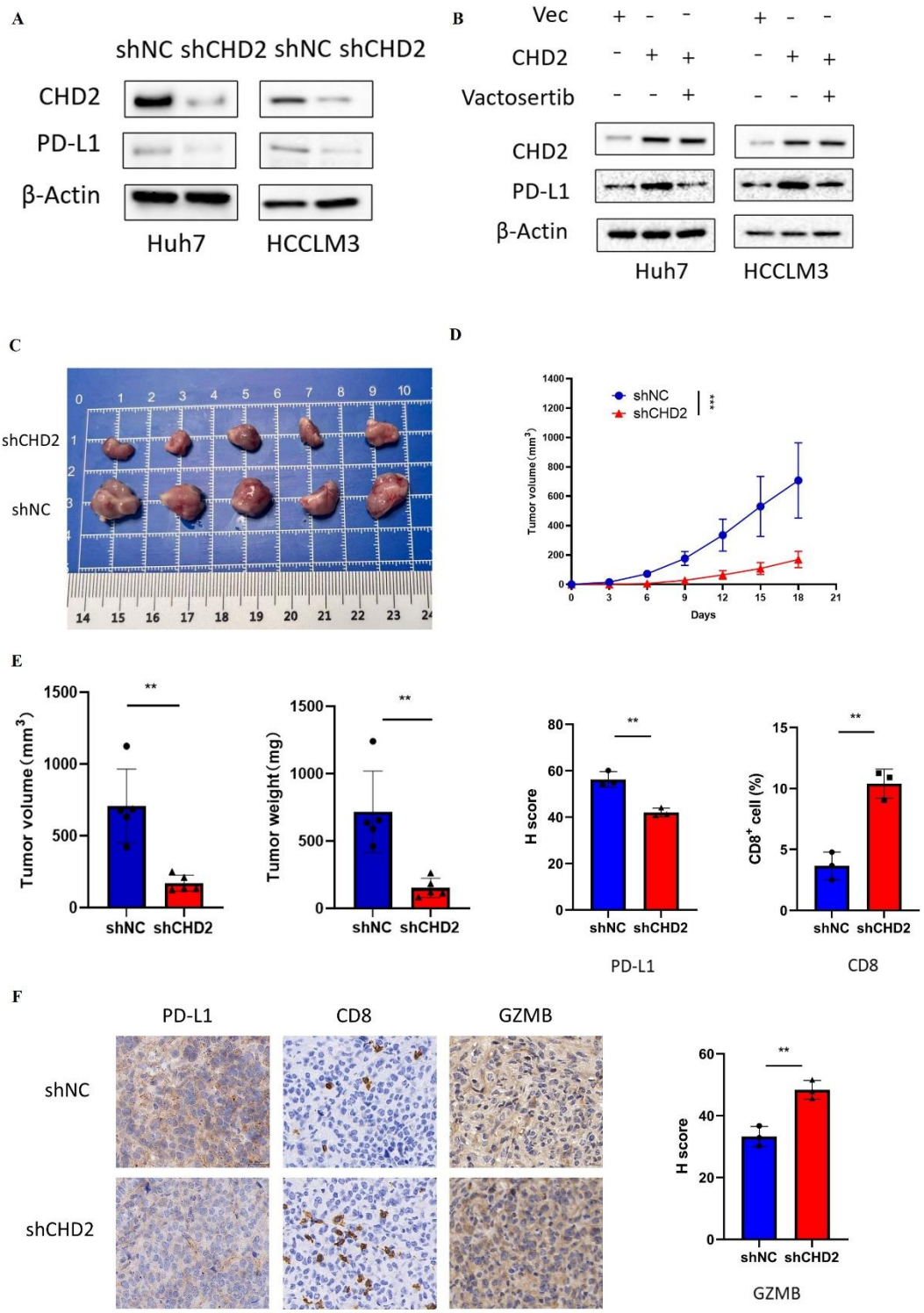


FIGURE 13 | CHD2 regulates the tumor immune microenvironment.(A) PD-L1 expression after CHD2 knockdown by western blot.(B) CHD2 overexpression promoted PD-L1 expression, which was reversed by Vactosertib treatment by western blot.(C–E) In vivo xenograft tumor growth analysis, including tumor growth curves and endpoint tumor weight.(F) Immunohistochemical staining of PD-L1, CD8, and GZMB.(**p < 0.01, ***p < 0.001)

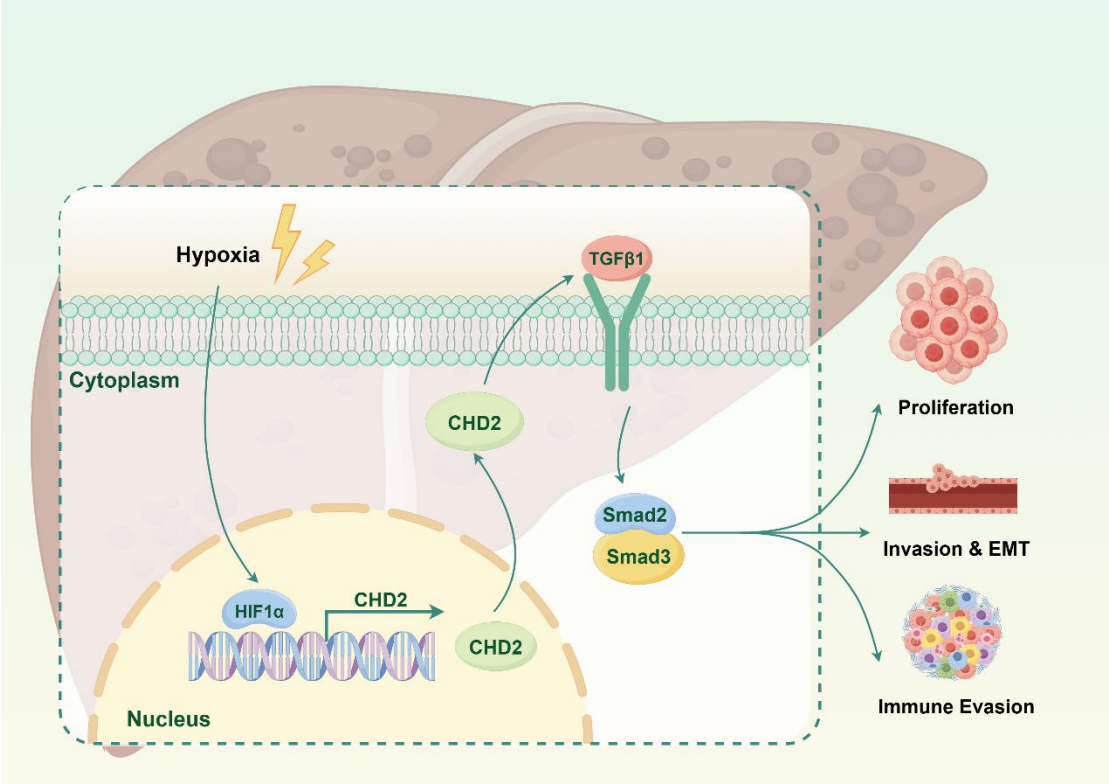


FIGURE 14 | Mechanism diagram by Figdraw.

Discussion

HCC remains one of the most aggressive cancers globally, with a five-year OS rate of less than 25%[4, 28]. The poor prognosis associated with HCC is attributed to its molecular heterogeneity and the lack of robust biomarkers for molecular stratification. Commonly used clinical indicators, such as alpha-fetoprotein (AFP) levels and TNM staging, exhibit limitations in reflecting the biological characteristics of the tumor, which make it difficult to accurately predict individual outcomes or guide precise therapies. Therefore, the identification of novel molecular biomarkers and their regulatory mechanisms is of critical importance for improving the clinical management of HCC.

In this study, CHD2 was upregulated across multiple independent cohorts, including TCGA, ICGC, and GEO datasets, which indicated that CHD2 levels were stable and reproducible across different cohorts. ROC analysis gave an AUC of 0.729, which demonstrated that CHD2 exhibited moderate diagnostic value for HCC. However, considering that a single biomarker is usually not enough for clinical diagnosis, CHD2 might work better as part of a multi-marker panel rather than as an independent diagnostic indicator. In addition, higher CHD2 expression was associated with worse OS, PFS, and DSS. This suggests that CHD2 may reflect more aggressive biological behavior. Furthermore, CHD2 was positively correlated with tumor-related functional states, such as EMT, proliferation, and immune evasion, which indicated that high CHD2 expression may represent increased malignant potential and

poorer clinical outcomes. These results suggest that CHD2 may be a biomarker for risk stratification and prognosis prediction in HCC patients.

Previous studies have generally characterized CHD2 as a tumor suppressor in several cancers. For example, loss of CHD2 function impairs chromatin remodeling-mediated DNA damage response signaling, thereby impairing genomic stability in lymphoma[29]. In gastric and colorectal cancers, CHD2 has a high mutation frequency, and truncating mutations may lead to loss of function and dysregulation of chromatin remodeling, which then contributes to tumorigenesis[30]. Nevertheless, the role of CHD2 has rarely been investigated in HCC. In contrast to previous reports that have described the tumor-suppressive functions of CHD2, our study for the first time demonstrates that CHD2 has oncogenic effects in HCC.

Previous studies have primarily focused on the role of CHD2 as a chromatin remodeling protein involved in transcriptional regulation and DNA structural maintenance. For example, PARP1 has been reported to recruit CHD2 to mediate chromatin expansion and histone deposition, which facilitated DNA double-strand break repair through non-homologous end joining (NHEJ)[31]. However, our study suggests that CHD2 is not only associated with intrinsic malignant phenotypes of tumor cells but is also involved in TME remodeling. High CHD2 expression in tumors correlated with greater infiltration by M2 macrophages and regulatory T cells. But effector immune cells infiltration, such as $CD8^+$ T cells and activated NK cells, was reduced. Correlation analyses indicated that CHD2 expression was positively associated with the TGF-β pathway and several immune-related chemokines and receptors, including CCR4, IL6R, and XCR1, suggesting that CHD2 may suppress antitumor immune responses by regulating immune cell recruitment and activating immunosuppressive signaling pathways. Moreover, CHD2 expression negatively correlated with several key steps of the cancer immunity cycle. Besides, our in vitro experiments showed that CHD2 upregulated PD-L1. Subcutaneous tumor models in C57BL/6 mice in vivo further confirmed that CHD2 expression positively correlated with PD-L1 expression, while negatively correlating with CD8 and GZMB expression. These findings further support the important role of CHD2 in shaping an immunosuppressive TME.

Mechanistically, by integrating predictive results from the hTFtarget, ChEA, and GTRD databases with hypoxia-related RNA-seq and ChIP-seq datasets, we propose that HIF1-α acts as a potential upstream regulator of CHD2 and is subject to hypoxic regulation. Positive correlations between HIF1-α and CHD2 were further observed in both single-cell and spatial transcriptomic datasets. Moreover, hypoxia treatment experiments confirmed that CHD2 expression responds to hypoxia stimulation. ChIP-qPCR assays further demonstrated the direct transcriptional regulation of CHD2 by HIF1-α. In the HCC microenvironment, persistent hypoxia induces the expression of HIF1-α, which functions as a transcription factor to activate multiple downstream genes. For example, HIF1-α has been reported to directly induce ABCB1 transcription, thereby promoting regorafenib efflux and drug resistance in HCC[32]. Our findings suggest that activation of CHD2 by HIF1-α under hypoxia may represent an important mechanism in HCC. Since the role of CHD2 as a hypoxia-responsive molecule has rarely

been reported, our findings further expand the upstream regulatory mechanism of CHD2.

The TGF-β/Smad pathway exerts pleiotropic and complex functions in HCC and plays critical roles in promoting angiogenesis, suppressing antitumor immunity, and regulating metabolic reprogramming, thereby facilitating tumor proliferation, invasion, and metastasis[8]. Through immune feature analyses, as well as KEGG and GSEA enrichment analyses from RNA-seq, we found that CHD2 expression was significantly associated with activation of the TGF-β signaling pathway. Single-cell and spatial transcriptomic analyses further demonstrated that CHD2 was predominantly enriched in malignant cells and exhibited co-localization and positive correlations with TGF-β1/3 and SMAD2/3, suggesting involvement of CHD2 in TGF-β/Smad pathway activation. Western blot results indicated that CHD2 knockdown markedly reduced TGF-β1/3 and phosphorylated Smad2/3. Furthermore, functional experiments demonstrated that the TGF-β receptor I inhibitor Vactosertib significantly reversed CHD2 overexpression-induced proliferation, invasion, EMT progression, and PD-L1 upregulation, further indicating that the TGF-β/Smad pathway functions as a critical downstream mediator of the oncogenic effects of CHD2.

Interestingly, although RNA-seq analysis, scRNA-seq, and functional experiments demonstrated that CHD2 promotes HCC progression by activating the TGF-β/Smad pathway, in silico knockout analysis by scTenifoldKnk revealed that genes perturbed following CHD2 depletion were enriched in pathways related to mitochondrial function, including oxidative phosphorylation, glycolysis, amino acid biosynthesis, and oxidative stress. This difference is mainly attributable to the distinct biological levels of different analytical approaches. From a methodological perspective, in silico knockout is based on gene regulatory networks inferred from scRNA-seq data. Its primary goal is to identify key transcriptional regulatory modules required for tumor cell survival. As a result, it is sensitive to fundamental cellular processes such as mitochondrial energy metabolism and intracellular redox balance. In contrast, signaling pathways such as TGF-β are regulated through multiple layers of control, including microenvironment-derived stimuli, intercellular paracrine signaling, and post-translational modifications of proteins. Therefore, changes in their activity are not always fully caught by changes in transcriptional network structure alone. Within this analytical framework, CHD2 depletion in the in silico knockout results is mainly reflected in disruptions of metabolism-related pathways. These findings suggest that CHD2 may play a foundational role in maintaining mitochondrial function and energy homeostasis in tumor cells.

Although our study describes the role of CHD2 in HCC, t several limitations should be acknowledged. First, our findings about the TME were mainly based on public databases, which may import potential selection bias. Second, although we demonstrated that CHD2 regulates proliferation, invasion, EMT, and PD-L1 expression through the TGF-β/Smad pathway, the underlying molecular mechanisms of regulation of TGF-β/Smad pathway by CHD2 require further investigation. In addition, the candidate therapeutic compound MK-886 identified in this study has not yet been validated, and its clinical applicability remains unknown.

In conclusion, our study systematically demonstrates that CHD2 is significantly upregulated in HCC and functions as a driver of tumor progression. High CHD2 expression is closely associated with poor prognosis and contributes to the formation of an immunosuppressive TME characterized by reduced infiltration of effector immune cells. Mechanistically, CHD2 is directly transcriptionally regulated by HIF1-α under hypoxia conditions and promotes HCC cell proliferation, EMT, invasion, metastasis, and PD-L1-mediated immune evasion through activation of the TGF-β/Smad signaling pathway. These findings were further validated by both in vitro and in vivo experiments. Overall, our study suggests that CHD2 serves as a biomarker and a potential therapeutic target in HCC. Although this study integrated multi-omics analyses with experimental validation, further clinical research and mechanism studies are still required to fully assess its translational potential and clinical value for improving HCC patient outcomes.

Acknowledgements

This study was supported by the Institutional Foundation of The First Affiliated Hospital of Xi'an Jiaotong University (No. 2025-QN-25).

Data Availability declaration

The data were available via corresponding authors for reasonable requires.

CRediT authorship contribution statement

Yichen Yang: Data curation, Investigation, Formal analysis, Software, Writing – original draft. **Bingyi Ren**: Data curation, Investigation. **Kai Sheng**: Data curation. **Zhiyuan Bai**: Investigation. **Yang Ren**: Investigation. **Yi Lv**: Supervision. **Kang Liu**: Conceptualization, Project administration, Funding acquisition, Validation, Writing – review and editing.

Conflict of Interest Statement

The authors declare no competing interests.

References

[1] B.M. Lehrich, S.P. Monga, WNT-β-catenin signalling in hepatocellular carcinoma: from bench to clinical trials, Nat Rev Gastroenterol Hepatol 23(3) (2026) 246-263.
[2] D. Hsiehchen, A.G. Singal, Hepatocellular carcinoma: Clinical trials to watch, Med 7(3) (2026)

101038.
[3] J.M. Llovet, R. Pinyol, S. Affo, M. Yarchoan, G.J. Gores, R.K. Kelley, S.W. Lowe, D. Sia, A. Villanueva, Hallmarks of liver cancer: Therapeutic implications, Cell 189(8) (2026) 2490-2514.
[4] M.V. Machado, Hepatocellular Carcinoma Around the Clock, Curr Oncol 33(1) (2026).
[5] J.C. Liu, C.G. Ferreira, T. Yusufzai, Human CHD2 is a chromatin assembly ATPase regulated by its chromo- and DNA-binding domains, J Biol Chem 290(1) (2015) 25-34.
[6] X. Zhang, S. Duan, P.E. Apostolou, X. Wu, J. Watanabe, M. Gallitto, T. Barron, K.R. Taylor, P.J. Woo, X. Hua, H. Zhou, H.J. Wei, N. McQuillan, K.D. Kang, G.K. Friedman, P.D. Canoll, K. Chang, C.C. Wu, R. Hashizume, C.R. Vakoc, M. Monje, G.M. McKhann, 2nd, J.A. Gogos, Z. Zhang, CHD2 Regulates Neuron-Glioma Interactions in Pediatric Glioma, Cancer Discov 14(9) (2024) 1732-1754.
[7] Z. Min, H. Xin, X. Liu, J. Wan, Z. Fan, X. Rao, J. Fan, L. Yang, D. Li, Chromodomain helicase DNA-binding domain 2 maintains spermatogonial self-renewal by promoting chromatin accessibility and mRNA stability, iScience 25(12) (2022) 105552.
[8] X. Xin, X. Cheng, F. Zeng, Q. Xu, L. Hou, The Role of TGF-β/SMAD Signaling in Hepatocellular Carcinoma: from Mechanism to Therapy and Prognosis, Int J Biol Sci 20(4) (2024) 1436-1451.
[9] J. Chen, W. Feng, M. Sun, W. Huang, G. Wang, X. Chen, Y. Yin, X. Chen, B. Zhang, Y. Nie, D. Fan, K. Wu, L. Xia, TGF-β1-Induced SOX18 Elevation Promotes Hepatocellular Carcinoma Progression and Metastasis Through Transcriptionally Upregulating PD-L1 and CXCL12, Gastroenterology 167(2) (2024) 264-280.
[10] Q. Ping, C. Wang, X. Cheng, Y. Zhong, R. Yan, M. Yang, Y. Shi, X. Li, X. Li, W. Huang, L. Wang, X. Bi, L. Hu, Y. Yang, Y. Wang, R. Gong, J. Tan, R. Li, H. Li, J. Li, W. Wang, R. Li, TGF-β1 dominates stromal fibroblast-mediated EMT via the FAP/VCAN axis in bladder cancer cells, J Transl Med 21(1) (2023) 475.
[11] H. Moses, M.H. Barcellos-Hoff, TGF-beta biology in mammary development and breast cancer, Cold Spring Harb Perspect Biol 3(1) (2011) a003277.
[12] S. Zhang, W.Y. Sun, J.J. Wu, W. Wei, TGF-β signaling pathway as a pharmacological target in liver diseases, Pharmacol Res 85 (2014) 15-22.
[13] S.Q. Sin, C.D. Mohan, R.M.W. Goh, M. You, S.C. Nayak, L. Chen, G. Sethi, K.S. Rangappa, L. Wang, Hypoxia signaling in hepatocellular carcinoma: Challenges and therapeutic opportunities, Cancer Metastasis Rev 42(3) (2023) 741-764.
[14] Y. Liu, Z. Xun, K. Ma, S. Liang, X. Li, S. Zhou, L. Sun, Y. Liu, Y. Du, X. Guo, T. Cui, H. Zhou, J. Wang, D. Yin, R. Song, S. Zhang, W. Cai, F. Meng, H. Guo, B. Zhang, D. Yang, R. Bao, Q. Hu, J. Wang, Y. Ye, L. Liu, Identification of a tumour immune barrier in the HCC microenvironment that determines the efficacy of immunotherapy, J Hepatol 78(4) (2023) 770-782.
[15] V. Thorsson, D.L. Gibbs, S.D. Brown, D. Wolf, D.S. Bortone, T.H. Ou Yang, E. Porta-Pardo, G.F. Gao, C.L. Plaisier, J.A. Eddy, E. Ziv, A.C. Culhane, E.O. Paull, I.K.A. Sivakumar, A.J. Gentles, R. Malhotra, F. Farshidfar, A. Colaprico, J.S. Parker, L.E. Mose, N.S. Vo, J. Liu, Y. Liu, J. Rader, V. Dhankani, S.M. Reynolds, R. Bowlby, A. Califano, A.D. Cherniack, D. Anastassiou, D. Bedognetti, Y. Mokrab, A.M. Newman, A. Rao, K. Chen, A. Krasnitz, H. Hu, T.M. Malta, H. Noushmehr, C.S. Pedamallu, S. Bullman, A.I. Ojesina, A. Lamb, W. Zhou, H. Shen, T.K. Choueiri, J.N. Weinstein, J. Guinney, J. Saltz, R.A. Holt, C.S. Rabkin, A.J. Lazar, J.S. Serody, E.G. Demicco, M.L. Disis, B.G. Vincent, I. Shmulevich, The Immune Landscape of Cancer, Immunity 48(4) (2018) 812-830.e14.
[16] A.M. Newman, C.L. Liu, M.R. Green, A.J. Gentles, W. Feng, Y. Xu, C.D. Hoang, M. Diehn, A.A.

Alizadeh, Robust enumeration of cell subsets from tissue expression profiles, Nat Methods 12(5) (2015) 453-7.
[17] D. Aran, Z. Hu, A.J. Butte, xCell: digitally portraying the tissue cellular heterogeneity landscape, Genome Biol 18(1) (2017) 220.
[18] E. Becht, N.A. Giraldo, L. Lacroix, B. Buttard, N. Elarouci, F. Petitprez, J. Selves, P. Laurent-Puig, C. Sautès-Fridman, W.H. Fridman, A. de Reyniès, Estimating the population abundance of tissue-infiltrating immune and stromal cell populations using gene expression, Genome Biol 17(1) (2016) 218.
[19] F. Finotello, C. Mayer, C. Plattner, G. Laschober, D. Rieder, H. Hackl, A. Krogsdam, Z. Loncova, W. Posch, D. Wilflingseder, S. Sopper, M. Ijsselsteijn, T.P. Brouwer, D. Johnson, Y. Xu, Y. Wang, M.E. Sanders, M.V. Estrada, P. Ericsson-Gonzalez, P. Charoentong, J. Balko, N. de Miranda, Z. Trajanoski, Molecular and pharmacological modulators of the tumor immune contexture revealed by deconvolution of RNA-seq data, Genome Med 11(1) (2019) 34.
[20] J. Racle, D. Gfeller, EPIC: A Tool to Estimate the Proportions of Different Cell Types from Bulk Gene Expression Data, Methods Mol Biol 2120 (2020) 233-248.
[21] D. Amara, D.M. Wolf, L. van 't Veer, L. Esserman, M. Campbell, C. Yau, Co-expression modules identified from published immune signatures reveal five distinct immune subtypes in breast cancer, Breast Cancer Res Treat 161(1) (2017) 41-50.
[22] F. Sanchez-Vega, M. Mina, J. Armenia, W.K. Chatila, A. Luna, K.C. La, S. Dimitriadoy, D.L. Liu, H.S. Kantheti, S. Saghafinia, D. Chakravarty, F. Daian, Q. Gao, M.H. Bailey, W.W. Liang, S.M. Foltz, I. Shmulevich, L. Ding, Z. Heins, A. Ochoa, B. Gross, J. Gao, H. Zhang, R. Kundra, C. Kandoth, I. Bahceci, L. Dervishi, U. Dogrusoz, W. Zhou, H. Shen, P.W. Laird, G.P. Way, C.S. Greene, H. Liang, Y. Xiao, C. Wang, A. Iavarone, A.H. Berger, T.G. Bivona, A.J. Lazar, G.D. Hammer, T. Giordano, L.N. Kwong, G. McArthur, C. Huang, A.D. Tward, M.J. Frederick, F. McCormick, M. Meyerson, E.M. Van Allen, A.D. Cherniack, G. Ciriello, C. Sander, N. Schultz, Oncogenic Signaling Pathways in The Cancer Genome Atlas, Cell 173(2) (2018) 321-337.e10.
[23] G.L. Semenza, Targeting HIF-1 for cancer therapy, Nat Rev Cancer 3(10) (2003) 721-32.
[24] T.M. Malta, A. Sokolov, A.J. Gentles, T. Burzykowski, L. Poisson, J.N. Weinstein, B. Kamińska, J. Huelsken, L. Omberg, O. Gevaert, A. Colaprico, P. Czerwińska, S. Mazurek, L. Mishra, H. Heyn, A. Krasnitz, A.K. Godwin, A.J. Lazar, J.M. Stuart, K.A. Hoadley, P.W. Laird, H. Noushmehr, M. Wiznerowicz, Machine Learning Identifies Stemness Features Associated with Oncogenic Dedifferentiation, Cell 173(2) (2018) 338-354.e15.
[25] C. Yang, H. Zhang, M. Chen, S. Wang, R. Qian, L. Zhang, X. Huang, J. Wang, Z. Liu, W. Qin, C. Wang, H. Hang, H. Wang, A survey of optimal strategy for signature-based drug repositioning and an application to liver cancer, Elife 11 (2022).
[26] D. Osorio, Y. Zhong, G. Li, Q. Xu, Y. Yang, Y. Tian, R.S. Chapkin, J.Z. Huang, J.J. Cai, scTenifoldKnk: An efficient virtual knockout tool for gene function predictions via single-cell gene regulatory network perturbation, Patterns (N Y) 3(3) (2022) 100434.
[27] R.M. Meyers, J.G. Bryan, J.M. McFarland, B.A. Weir, A.E. Sizemore, H. Xu, N.V. Dharia, P.G. Montgomery, G.S. Cowley, S. Pantel, A. Goodale, Y. Lee, L.D. Ali, G. Jiang, R. Lubonja, W.F. Harrington, M. Strickland, T. Wu, D.C. Hawes, V.A. Zhivich, M.R. Wyatt, Z. Kalani, J.J. Chang, M. Okamoto, K. Stegmaier, T.R. Golub, J.S. Boehm, F. Vazquez, D.E. Root, W.C. Hahn, A. Tsherniak, Computational correction of copy number effect improves specificity of CRISPR-Cas9 essentiality screens in cancer cells, Nat Genet 49(12) (2017) 1779-1784.

[28] M.A. Butt, E.S. Aby, J.D. Debes, The global epidemiology of hepatocellular carcinoma, Hepatol Commun 10(5) (2026).
[29] P. Nagarajan, T.M. Onami, S. Rajagopalan, S. Kania, R. Donnell, S. Venkatachalam, Role of chromodomain helicase DNA-binding protein 2 in DNA damage response signaling and tumorigenesis, Oncogene 28(8) (2009) 1053-62.
[30] M.S. Kim, N.G. Chung, M.R. Kang, N.J. Yoo, S.H. Lee, Genetic and expressional alterations of CHD genes in gastric and colorectal cancers, Histopathology 58(5) (2011) 660-8.
[31] M.S. Luijsterburg, I. de Krijger, W.W. Wiegant, R.G. Shah, G. Smeenk, A.J.L. de Groot, A. Pines, A.C.O. Vertegaal, J.J.L. Jacobs, G.M. Shah, H. van Attikum, PARP1 Links CHD2-Mediated Chromatin Expansion and H3.3 Deposition to DNA Repair by Non-homologous End-Joining, Mol Cell 61(4) (2016) 547-562.
[32] B. Tao, C. Yi, B. Zhang, Y. Geng, Y. Gu, R. Sun, X. Wang, J. Lin, J. Chen, ERBB3 blockade sensitizes hepatocellular carcinoma to regorafenib after first-line tyrosine kinase inhibitor resistance by inhibiting HIF1A-ABCB1 signaling, Clin Mol Hepatol 32(2) (2026) 787-807.

Supplementary Files

This is a list of supplementary files associated with this preprint. Click to download.

- figureS1.jpg
- figureS2.jpg
- figureS3.jpg
- figureS4.jpg
- figureS5.jpg
- figureS6.jpg